Cell Reports
Physical Science

CellPress
OPEN ACCESS

Article

A carbon-efficient bicarbonate electrolyzer

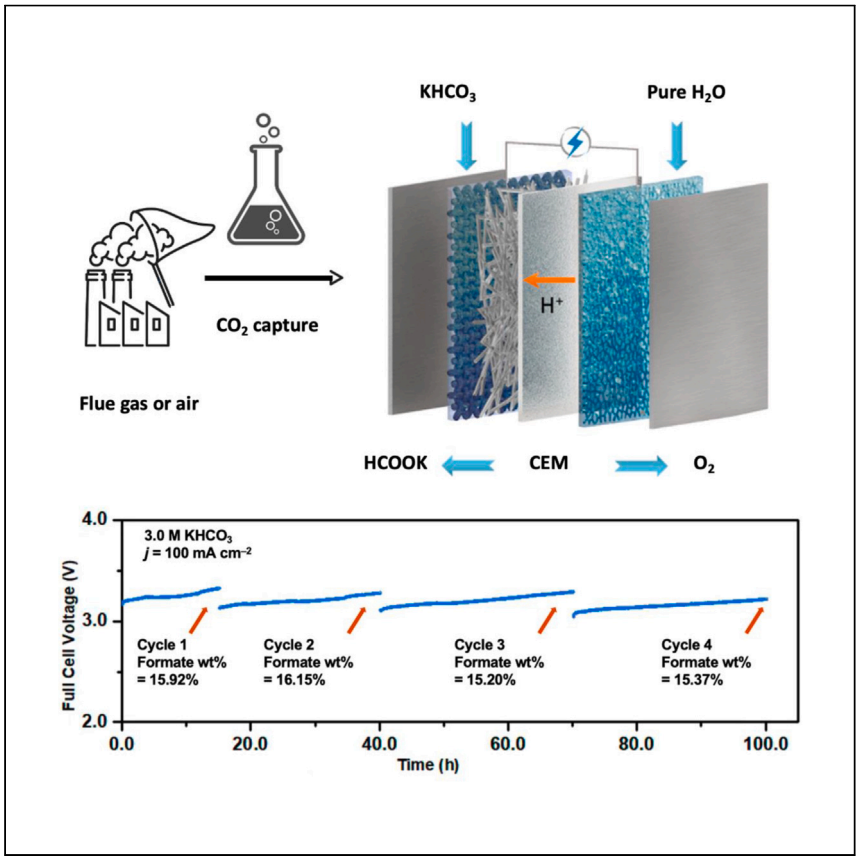

Zhang et al. design a bicarbonate electrolyzer to couple carbon dioxide capture with carbon dioxide electroreduction. With careful pH and partial pressure engineering, and the adoption of a cation exchange membrane and intermediate layer, aqueous bicarbonate feedstock is converted into solid formate fuel with a high carbon efficiency.

Zhen Zhang, Dawei Xi, Zhichu Ren, Ju Li

liju@mit.edu

Highlights

Impacts of CO_2 partial pressure on local pH and carbon efficiency are gauged

CO_2, bicarbonate, and carbonate equilibrium are key to achieving high carbon efficiency

Bicarbonate-to-formate electrochemical conversion generates no net acid or base

Formate is a potential solid fuel for seasonal energy storage

Zhang et al., Cell Reports Physical Science 4, 101662
November 15, 2023
https://doi.org/10.1016/j.xcrp.2023.101662

Please cite this article in press as: Zhang et al., A carbon-efficient bicarbonate electrolyzer, Cell Reports Physical Science (2023), https://doi.org/10.1016/j.xcrp.2023.101662

Cell Reports
Physical Science

Article

A carbon-efficient bicarbonate electrolyzer

Zhen Zhang,[1] Dawei Xi,[2] Zhichu Ren,[1] and Ju Li[1,3,4,*]

SUMMARY

Carbon efficiency is one of the most pressing problems of carbon dioxide electroreduction today. While there have been studies on anion exchange membrane electrolyzers with carbon dioxide (gas) and bipolar membrane electrolyzers with bicarbonate (aqueous) feedstocks, both suffer from low carbon efficiency. In anion exchange membrane electrolyzers, this is due to carbonate anion crossover, whereas in bipolar membrane electrolyzers, the exsolution of carbon dioxide (gas) from the bicarbonate solution is the culprit. Here, we first elucidate the root cause of the low carbon efficiency of liquid bicarbonate electrolyzers with thermodynamic calculations and then achieve carbon-efficient carbon dioxide electroreduction by adopting a near-neutral-pH cation exchange membrane, a glass fiber intermediate layer, and carbon dioxide (gas) partial pressure management. We convert highly concentrated bicarbonate solution to solid formate fuel with a yield (carbon efficiency) of greater than 96%. A device test is demonstrated at 100 mA cm^{-2} with a full-cell voltage of 3.1 V for over 200 h.

INTRODUCTION

Carbon dioxide electroreduction (CO_2ER) is an attractive strategy of CO_2 utilization for providing various chemicals (HCOOH, CO, C_2H_4, CH_3COOH, C_2H_5OH, etc.) while decreasing atmospheric CO_2 simultaneously.[1,2] Over the past 40 years, considerable progress has been made in developing numerous types of catalysts to improve the Faradaic efficiency (FE) for CO_2ER relying on a CO_2(gas) feedstock. However, the technology is still far from industrialization because of multiple critical challenges.[3–7] In particular, carbon efficiency, which is the percentage of CO_2 utilized among the captured, is one of the most basic and pressing issues that impedes the commercialization of CO_2 electrolyzers today.[8] For many traditional anion exchange membrane (AEM) CO_2 electrolyzers, the carbon efficiency is typically below 10%,[6] while a carbon efficiency of over 80% is required for the commercialization of CO_2ER.[9]

Traditionally, CO_2 capture and CO_2ER have been considered separately.[10] CO_2 captured from dilute sources should be first converted (typically to solid calcium carbonate, $CaCO_3$), transported, thermally decomposed, and pressurized to become ultra-pure CO_2 gas feedstock (Figure S1).[11,12] For the prevalent alkaline- or neutral-medium-based aqueous membrane electrode assembly (MEA) electrolyzers, over 50% of the capital cost would come from this solid-state thermal regeneration process[4,9] which is highly energy intensive.[13] In addition, in the aqueous environment, CO_2ER involves proton-coupled electron transfer (PCET) reactions, locally generating hydroxides (e.g., $CO_2 + H_2O + 2e^- \rightarrow CO + 2OH^-$). The OH^- ions would have a chance to convert reactive CO_2* into electrochemically inert CO_3^{2-}(aq) ($2OH^- + CO_2 \rightarrow CO_3^{2-} + H_2O$), which is a "trap state" in the catholyte.[14–17] In

[1]Department of Materials Science and Engineering, Massachusetts Institute of Technology, Cambridge, MA 02139, USA

[2]John A. Paulson School of Engineering and Applied Sciences, Harvard University, Cambridge, MA 02138, USA

[3]Department of Nuclear Science and Engineering, Massachusetts Institute of Technology, Cambridge, MA 02139, USA

[4]Lead contact

*Correspondence: liju@mit.edu

https://doi.org/10.1016/j.xcrp.2023.101662

Please cite this article in press as: Zhang et al., A carbon-efficient bicarbonate electrolyzer, Cell Reports Physical Science (2023), https://doi.org/10.1016/j.xcrp.2023.101662

a CO_2 MEA electrolyzer with the AEM, HCO_3^-/CO_3^{2-} ions are the major charge carriers in the electrolyte and would cross over the membrane to the anode side with a high chance of being wasted (Figure S2a).[8,18] This carbon efficiency loss problem is more detrimental to products with more electrons transferred. For instance, for the 2-electron-transfer reaction of CO production, 2 OH^- ions are generated per 1 CO_2 converted, and thus the carbon efficiency loss will be 50%, assuming all $OH^- \rightarrow CO_3^{2-}$ will drift across and get lost. For the 6-electron-transfer reaction of C_2H_5OH production, 6 OH^- ions are generated per 1 CO_2 converted, and thus the efficiency loss will be 75% (Table S1).[19] Further, the parasitic hydrogen evolution reaction (HER) also produces OH^- ($2H_2O + 2e^- \rightarrow H_2 + 2OH^-$), which further lowers the carbon efficiency and FE. Until today, most of the reported CO_2ER research *only* accounts for the percentage of CO_2 actually converted, but it leaves out the substantial amount of CO_2 unconverted or wasted, which is either lost as crossover CO_3^{2-}/HCO_3^- or just unreacted and merges into a gaseous mixture with the outlet products. Thus, the combined carbon efficiency and energy efficiency of CO_2 capture and electroreduction, through the traditional route with solid $CaCO_3$ and ultrapure gaseous CO_2, is very low.[11,12]

To address this critical challenge, rather than relying on the CO_2(gas) feedstock, bipolar membrane (BPM) electrolyzers with *aqueous* bicarbonate HCO_3^-(aq) input were demonstrated (Figure S2b).[11,15,20,21] In principle, the energy-intensive CO_2 regeneration process could be circumvented. In practice, however, the BPM induces a large overpotential, causing low energy efficiency, and it still suffers from CO_2 escape, low FE, low yield, and low operation lifetime. The carbon efficiency problem is due to the thermodynamically driven CO_2 outgassing from a highly concentrated bicarbonate feedstock. Carbonate ions would be produced spontaneously ($2HCO_3^- \rightleftharpoons CO_2$(out gas) + $CO_3^{2-} + H_2O$), which suppresses both the FE and carbon efficiency. Here, we note the retention of relatively low pH is crucial, as H^+(aq) is a promoter of CO_2ER in bicarbonate electrolyzers. H^+(aq) converts inactive HCO_3^- into reactive CO_2. Further, H^+(aq) balances solution pH, which is crucial to achieving a high carbon efficiency. During operation, reactions that lead to net base production, such as CO production from HCO_3^- (full reaction: $HCO_3^- \rightarrow CO + ½\ O_2 + OH^-$), would pile up deleterious CO_3^{2-}(aq) and OH^-(aq), buffering the feedstock, impeding its further operation. Thereupon, the conversion of bicarbonate is restricted. Consequently, the selectivity of CO_2ER would decline continuously in constant-current mode, as we will show.

RESULTS AND DISCUSSION

Thermodynamic analysis

We first identify the key causes of the carbon efficiency loss in liquid *bicarbonate* electrolyzers with the Pourbaix diagram (Figure 1A). "No net acid or base production" is essential to maintaining a steady pH and high yield (carbon efficiency). In a bicarbonate electrolyzer, the electrochemical CO_2ER is preceded by *in situ* CO_2* generation from HCO_3^-(aq) as follows:

$$xHCO_3^-(aq) + xH^+(aq) \rightarrow xCO_2^* + xH_2O(aq) \quad \text{(Equation 1)}$$

$$xCO_2^* + ze^- + nH^+(aq) \rightarrow (C_xH_{n-2y}O_{2x-y})^{n-z}(aq) + yH_2O(aq) \quad \text{Equation 2}$$

From the Nernst equation, the slope of the electrochemical reaction above could be expressed as $k = -nRT/zF \ln 10$, where n and z are the number of protons and electrons transferred in the reaction, respectively. In particular, for the cation exchange membrane (CEM) configuration with a water anode, z is also the number

Please cite this article in press as: Zhang et al., A carbon-efficient bicarbonate electrolyzer, Cell Reports Physical Science (2023), https://doi.org/10.1016/j.xcrp.2023.101662

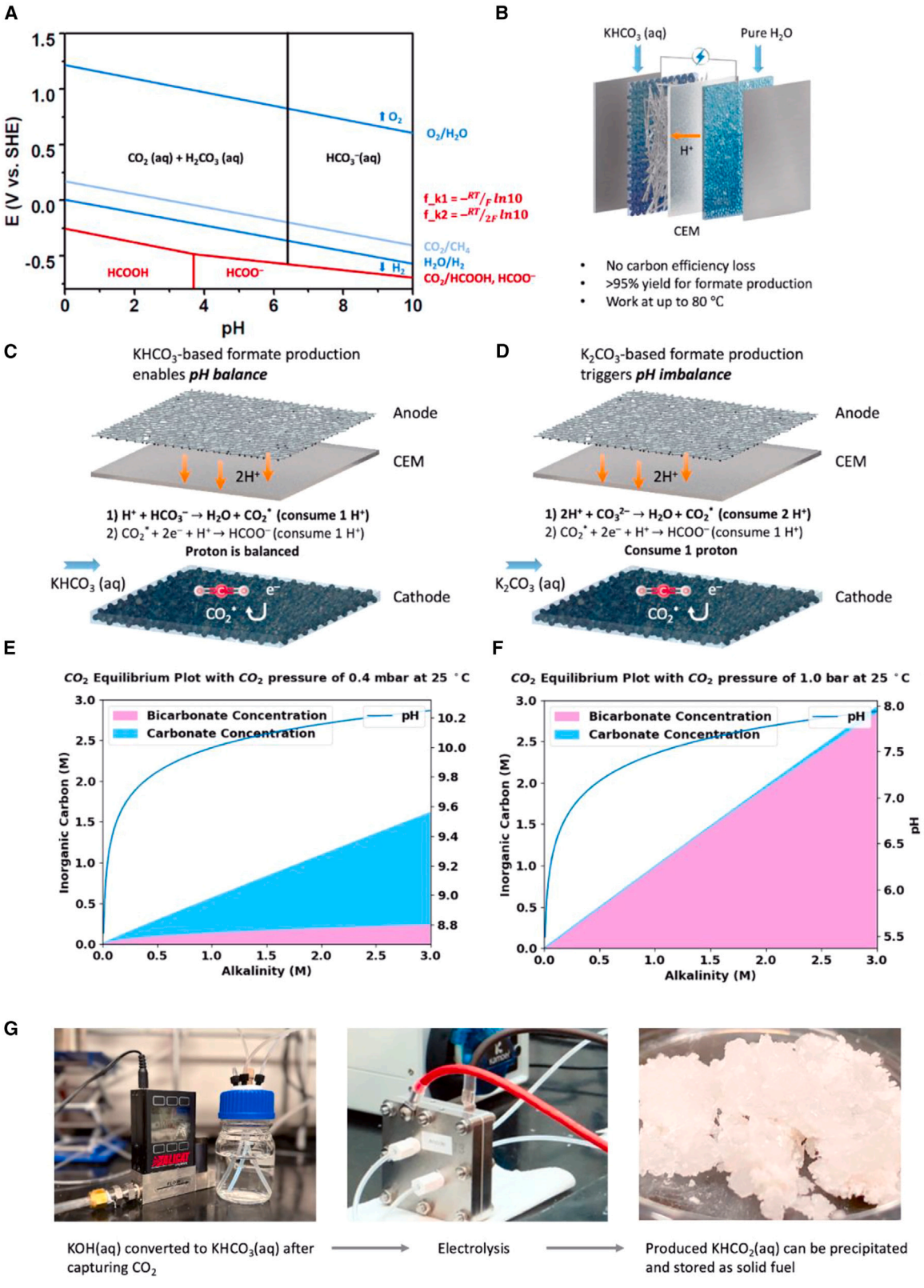

Figure 1. Pragmatic overview and design principles of the carbon-neutral complete electrochemical conversion from bicarbonate to solid formate fuel achieved in this work

(A) The Pourbaix diagram of representative CO_2 reduction (CO_2R) reactions in aqueous bicarbonate solutions at standard conditions. All the reactions are considered with respect to CO_2 molecules, because CO_2* is currently considered as a reactan. For instance, the two segments of formic acid and formate production reactions are $CO_2 + 2e^- + 2H^+ \rightarrow HCOOH$ and $CO_2 + 2e^- + H^+ \rightarrow HCOO^-$, respectively. From the Nernst equation, when the number of electron and proton transfers is the same, the slope of the curve should be $-(RT/F\ln 10)$. The acidic dissociation constant of formic acid is 1.77×10^{-4}. The bicarbonate-phase region was divided from a pH of 6.36. Beyond pH of 10.25, carbonate dominates, and that region is not of interest in this work. f_k1 and f_k2 refer to the slopes of the formic acid and formate formation, respectively.

(B) Schematic of the low overpotential cation exchange membrane (CEM) electrolyzer with a buffer layer using the liquid bicarbonate feedstock.

(C and D) The mechanism of the elimination of carbon efficiency loss and realization of complete yield of formate from bicarbonate. Comparison of mechanisms for proton-coupled electron transfer (PCET) reactions based on pure (C) bicarbonate and (D) carbonate feedstock. Pure bicarbonate feedstock would ensure proton balance, while pure carbonate would cause net proton consumption.

(E and F) The concentrations of inorganic carbon (HCO_3^-/CO_3^{2-}) and pH as a function of alkalinity when the solution is in equilibrium with a CO_2 partial pressure P_{CO2} in the gaseous overhead space of (E) 0.4 mbar and (F) 1 bar, respectively. Plum and light sky-blue areas correspond to the HCO_3^-(aq) and CO_3^{2-}(aq) concentrations, respectively.

(G) Optical photographs of the capture and conversion processes of solid formate production. CO_2 is absorbed by KOH, intermediated by $KHCO_3$, and electrochemically converted into high-purity formate solid with high yield, which could be used for fuel cells.

of protons shuttled from the anode side to the cathode side to complete the internal circuit. Therefore, three scenarios can occur:

Net acid (H^+) production:

$$z > x+n, \text{or } k > -nRT/(x+n)F \ln 10 \quad \text{(Equation 3)}$$

pH intrinsically balanced:

$$z = x+n, \text{or } k = -nRT/(x+n)F \ln 10 \quad \text{(Equation 4)}$$

Net base (OH^-) production:

$$z < x+n, \text{or } k < -\frac{nRT}{(x+n)F} \ln 10, \quad \text{(Equation 5)}$$

where k is the voltage vs. pH slope of a reaction equilibrium line on the Pourbaix diagram.

In particular, for CO_2ER to methane, alcohol, and CO, etc., z equals n (which also means $z < x + n$), the slope k is $-RT/F \ln 10$, and net base would be produced. Thus, these reactions would intrinsically cause the chemical equilibrium to shift toward the "trap state" of CO_3^{2-}(aq) formation ($OH^- + HCO_3^- \rightarrow CO_3^{2-} + H_2O$), which is highly electrochemically inert for CO_2ER. Further, the slope of CO_2ER to methane, alcohol, and CO is pH independent because these molecules would not readily shed protons under the operating conditions. However, weak acids such as formic acid (HCOOH) and acetic acid (CH_3COOH) would readily shed protons above a certain pH. Consequently, the slope in the Pourbaix diagram would become less negative. Specifically, we identified that for formate production, $z = x + n = 2$, and the slope is $-RT/2F \ln 10$, which indicates the reaction is pH balanced intrinsically, and thus, long-term operation can be maintained. Guided by this general principle of "no pH drift," we identified formate production to be the target steady-state reaction with CEM, where we should expect a theoretical carbon efficiency of 100%. Indeed, the full-cell reaction thus identified

$$KHCO_3 \rightarrow KOOCH + \tfrac{1}{2}O_2, \Delta H_f^\circ = 3.13 \text{ eV} \quad \text{(Equation 6)}$$

is analogous to water electrolysis,

$$H_2O \rightarrow H_2 + \tfrac{1}{2}O_2, \Delta H_f^\circ = 2.96 \text{ eV} \quad \text{(Equation 7)}$$

which is also pH balanced, and thus our metal-formate product KOOCH can be considered "solid hydrogen" fuel that can be produced in steady-pH

configuration. Throughout this work, we demonstrated the electrochemical reactions in device-level MEA electrolyzers (Figure 1B). We employed a CEM, pure bicarbonate feedstock and commercially available tin nanoparticle catalysts.

Although CO_2(aq), HCO_3^-(aq), and CO_3^{2-}(aq) are often considered to be in the same family, their carbon centers are different in terms of electrophilicity, and thus, the microscopic reaction pathways are different. We believe in order for electroreduction to occur, CO_2(aq)/HCO_3^-(aq)/CO_3^{2-}(aq) need to be first converted into CO_2*, the surface-adsorbed intermediate at the electrocatalyst/aqueous solution interface before electron transfer from the cathode can occur. Theoretically, using a CEM, the production of formate from pure HCO_3^-(aq) solution would not alter the catholyte pH (Figure 1C). This is because for every formate molecule generated, two protons would be consumed, while exactly two protons would migrate through the CEM. However, if we consume CO_3^{2-}(aq) by first combining with $2H^+$(aq) to form CO_2*, the generation of each formate molecule would result in the net production of 1 OH^- in the catholyte, thus leading to a carbon efficiency loss of 33% (Figure 1D). The continuous increasing of the concentrations of CO_3^{2-}/OH^- triggers a vicious cycle, and the FE/selectivity would plummet drastically, ultimately leading to exclusive HER. Following the net reaction of $KHCO_3 \rightarrow KOOCH + \frac{1}{2}O_2$, avoiding net acid or base accumulation that ultimately leads to HER is crucial.[22] The question arises as to how to maintain a high concentration of HCO_3^-(aq) while suppressing CO_3^{2-}(aq) concentration. And since the maintenance of pH in a specific region to avoid the CO_3^{2-}(aq) deep trap is essential, this also calls for a specific initial catholyte pH and CEM.

The concentrations of inorganic carbon species (CO_2/HCO_3^-/CO_3^{2-}) in equilibrium with different atmospheres were computed and plotted against alkalinity, which, as a convention,[23,24] denotes the concentration of the conserved cations (K^+, Na^+, Ca^{2+}, etc.) in the solution (Figures 1E, 1F, and S3). It is shown that in equilibrium with ambient air where the CO_2 partial pressure is 400 ppm (roughly 0.4 mbar), carbonate species dominate: [CO_3^{2-}(aq)] >> [HCO_3^- (aq)] (Figure 1E). This means that a freshly prepared bicarbonate solution would *thermodynamically* exude CO_2 (gas) in contact with normal air, resulting in a mixture of HCO_3^-(aq)/CO_3^{2-}(aq), which suffers enormously from the carbon-efficiency problem stated above and becomes almost inert for CO_2ER at some point. This is because CO_3^{2-}(aq) is directly inert toward CO_2ER and must consume $2H^+$(aq) to boost its reactivity. However, when the partial pressure of CO_2 in the overhead gas, P_{CO2}, reaches 1 atm and above, bicarbonate dominates in the aqueous phase: [HCO_3^-(aq)] $\gg$ [CO_3^{2-}(aq)] (Figure 1F). This means that the freshly prepared bicarbonate feedstock could be converted into formate with a theoretical yield of ~100% with nearly zero carbon efficiency loss, if in a constant CO_2 partial pressure environment of P_{CO2} = 1 atm or higher. No continuous external CO_2 gas source is required; only a small quantity of CO_2(gas) initially filling up the container headspace would be sufficient.

The key is therefore the maintenance of steady-state H^+(aq) concentration, and this excludes the use of a single AEM in bicarbonate electrolyzers. Instead, we use near-neutral (pH = 5–7, with local pH near the anode being even more acidic) water anolyte and CEM. The advance of our strategy is the maintenance of steady-state acidity throughout the entire process of PCET-based bicarbonate electrolysis, which is achieved by the integration of a low-resistance CEM and the balance of the CO_2 dissolution-exsolution equilibrium. Consequently, CO_2 (even from dilute sources) could also be absorbed efficiently by hydroxide to form bicarbonate, which could

Please cite this article in press as: Zhang et al., A carbon-efficient bicarbonate electrolyzer, Cell Reports Physical Science (2023), https://doi.org/10.1016/j.xcrp.2023.101662

be directly converted into formate with a yield of >95%, quantified with nuclear magnetic resonance (NMR) (Figures 1G and S4).

At scale, our strategy fits well into the global framework of carbon capture, utilization, and sequestration (CCUS). Various alkali basalt mineral rocks, containing CaO, MgO, SiO_2, Na_2O, and K_2O, were found in abundance on Earth and used for enhanced weathering.[25] They are efficient for removing CO_2 from the atmosphere and would form carbonates and bicarbonates.[25,26] The insoluble components could be separated and buried for carbon sequestration, while the soluble components, containing potassium, sodium, and calcium, etc., with our method, could be converted electrochemically into energy-rich metal-formate fuels (Figure 1G) for seasonal energy storage. A direct formate fuel cell (DFFC) possesses a high volumetric energy density (53g H_2 per liter) and high specific energy density (2.13 kWh kg^{-1}, more than 5 times that of the state-of-the-art lithium-ion batteries). Currently, a state-of-the-art DFFC demonstrated a peak power density of 302 mW cm^{-2}, which is already quite competitive against the standard H_2 PEM (proton-exchange membrane) fuel cell (~700 mW cm^{-2}),[27] thus opening the door for seasonal or even multi-year storage of the intermittent wind and solar electricity.

Proof of concept

As a proof-of-concept experiment, we intended to first demonstrate that dilute (0.1 M) bicarbonate feedstock can be ~100% converted. We used a freshly prepared 0.1 M $KHCO_3$ solution and filled the sealed solvent bottle headspace with CO_2 gas. There was no external CO_2 gas input during the electrolysis. After 7 h of electrolysis, we converted 94.60% of the $KHCO_3$ to KOOCH (Figures 2A, 2C, and S5). The produced formate concentration is around 94.6 mM, far exceeding the solubility of CO_2 (33 mM), and whose absolute quantity is also much greater than the small amount of the overhead CO_2 gas. Experimentally, this proved that the formate was converted from aqueous bicarbonate. This conclusion can also be inspected from the law of charge balance in the electrolyte. In our system, the catholyte is $KHCO_3$, while the anolyte is pure H_2O. Thus, the K^+ concentration is fixed (There is no obvious volume change of the solution before and after the electrolysis). The catholyte pH before and after the electrolysis ranged from 6 to 7, and thus both the $[H^+]$ and $[OH^-]$ concentrations are very low compared with K^+. Therefore, the positive charge carried by the K^+ has to be balanced by HCO_2^-, HCO_3^-, and CO_3^{2-} anions. As the HCO_2^- concentration can be measured with NMR, we can thus know the concentration of HCO_3^- + CO_3^{2-}. In fact, the concentration of HCO_3^- and CO_3^{2-} can also be computed from the pH of the solution. This result was quantified and confirmed with both liquid-phase NMR (Figure 3D) and solid-phase X-ray diffraction after evaporation-induced precipitation (Figure 3E). Consequently, the aqueous CO_2 feedstock was nearly completely converted into solid formate fuel, with almost 100% carbon efficiency, at ambient pressure and temperature. This also means that CO_2 capture can be seamlessly integrated with CO_2 electroreduction through the bicarbonate intermediate (in either highly concentrated liquid form, or 2-phase saturated liquid + solid-precipitate form after exceeding the solubility limit) (Figure 1), without going through the energy-consuming $CaCO_3$ baking and gas compression[11] processes. We then used a 0.1 M $KHCO_3$ solution at pH ~ 9 (slightly higher initial pH than fresh solution) to compare. The solution had been aged for 1 day to reach pH 9 and recirculated the catholyte in open-air atmosphere during the electrolysis in the MEA electrolyzer (Figure 2B). Even after 12 h of electrolysis, the yield of formate is only 6%, demonstrating an FE of 0.58%. The pH of the solution was roughly constant before and after the electrolysis, because the CEM configuration ensures pH balance even for exclusive HER.

Please cite this article in press as: Zhang et al., A carbon-efficient bicarbonate electrolyzer, Cell Reports Physical Science (2023), https://doi.org/10.1016/j.xcrp.2023.101662

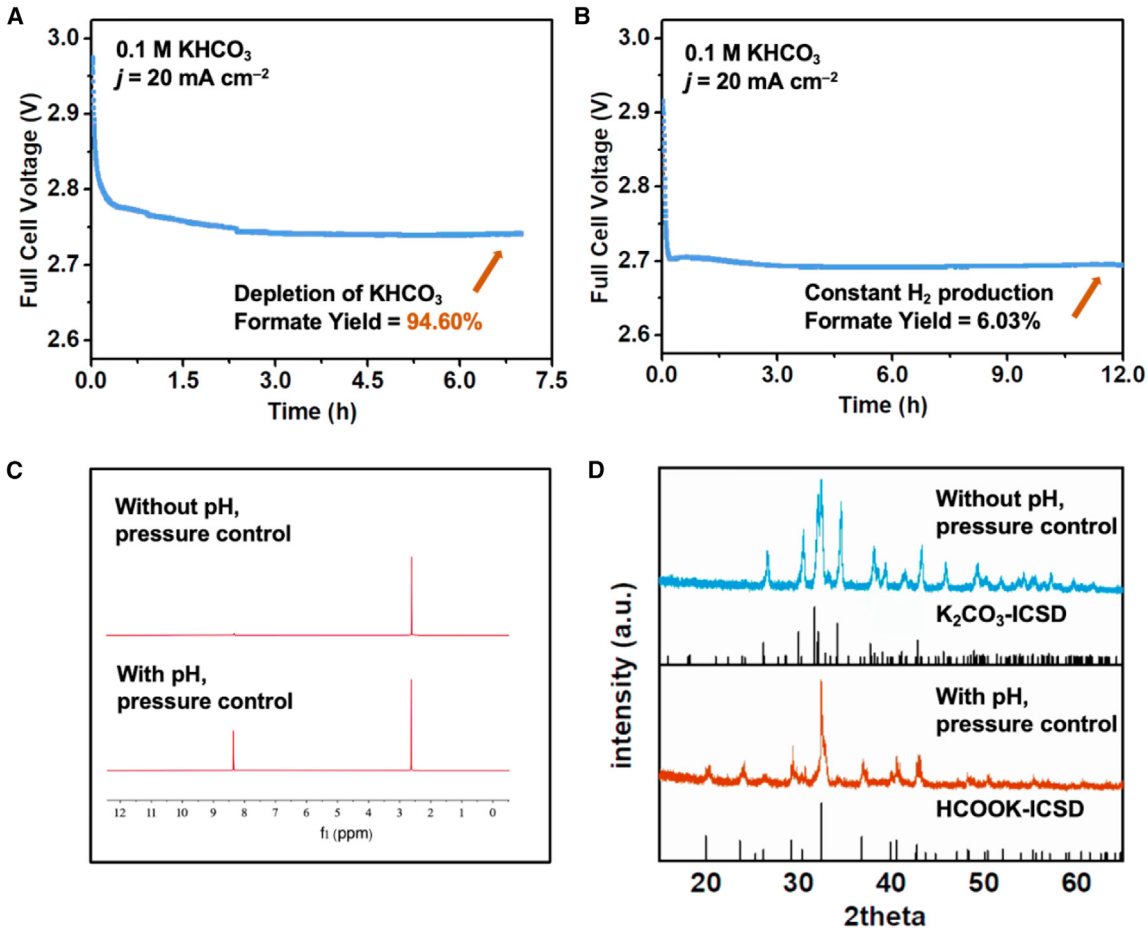

Figure 2. Proof-of-concept experiments in the membrane electrode assembly (MEA) electrolyzer

(A and B) Full-cell voltage as a function of time for 0.1 M $KHCO_3$ at 20 mA cm^{-2} (A) with and (B) without pH and pressure control. Almost pure competitive H_2 production occurred in the cathode chamber in the case of (A), while $KHCO_3$ was depleted after 7 h of electrolysis, yielding 94.60% of formate with a weight percent of 0.80% in the case of (B).

(C) NMR plots of the catholyte in (A) and (B), quantifying the concentration of formate.

(D) XRD patterns of solid products crystallized from catholytes in (A) and (B), compared with standard materials K_2CO_3 and HCOOK from database.

However, the solution was still unreactive as a mixture of HCO_3^-(aq) and CO_3^{2-}(aq). This highlights the importance of the initial pH for bicarbonate reduction.

Optimizing bicarbonate-to-formate electrolyzer

We further optimized the formate selectivity with cathode/electrolyte interface engineering. A hydrophobic gas diffusion layer carbon substrate would not be favorable for the mass transport of the liquid feedstock, and herein, a plain acid-etched hydrophilic carbon cloth was found to be more efficient, consistent with previous reports (Figure S6).[6,30,31] We also found that too strong an acidity at the cathode interface would favor HER. This was supported by comparing the situations of changing the anolyte to be a strong acid (0.1 M H_2SO_4) and deionized water or by adding an artificial glass fiber buffer layer.[32] Although the use of acids ensured superior ionic conductivity, the FE was below 3% (Figure S7) due to significant H^+ activity at the cathode and H_2(gas) evolution. Thus, we used a near-neutral-pH water anolyte and a bicarbonate-impregnated buffer layer between the cathode and CEM. The buffer layer could neutralize protons shuttling directly from the anode side, reducing over-acidity at the cathode/electrolyte surface, thus preventing severe HER. This

CellPress
OPEN ACCESS

Cell Reports
Physical Science
Article

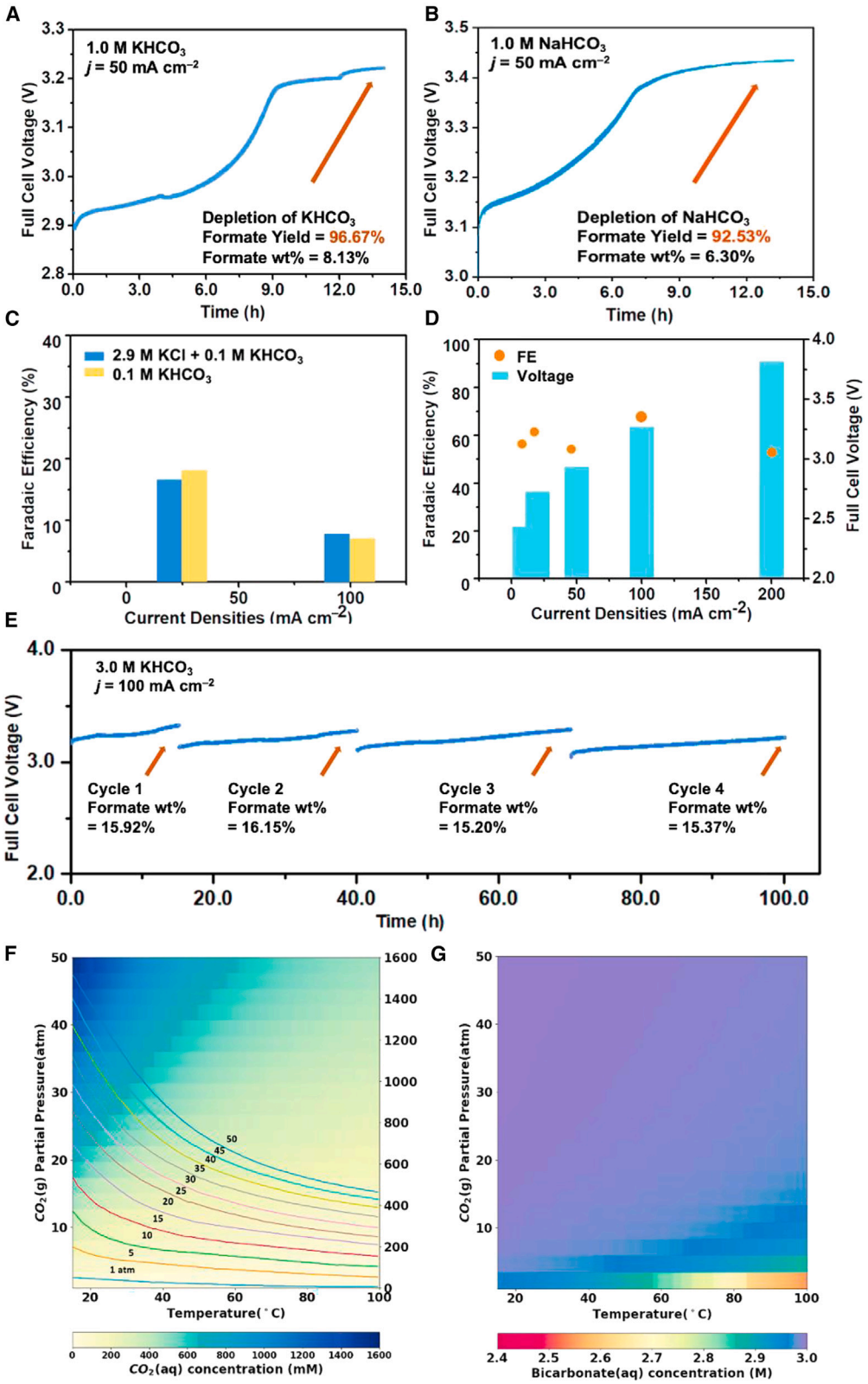

Please cite this article in press as: Zhang et al., A carbon-efficient bicarbonate electrolyzer, Cell Reports Physical Science (2023), https://doi.org/10.1016/j.xcrp.2023.101662

Figure 3. Electrochemical performance of high-yield formate production from bicarbonate feedstock in the membrane electrode assembly (MEA) electrolyzer

(A) Full-cell voltage as a function of time for 1.0 M $KHCO_3$ at 50 mA cm^{-2}. $KHCO_3$ was depleted after 14 h of electrolysis, yielding 96.67% of formate with 8.13 wt %.

(B) Full-cell voltage as a function of time for 1.0 M $NaHCO_3$ at 50 mA cm^{-2}. $KHCO_3$ was largely depleted after 14 h of electrolysis, yielding 92.53% of formate with 6.30 wt %.

(C) Cation effect exploration at the same bicarbonate concentration.

(D) FE of formate/full-cell voltage at different current densities after 1 h of electrolysis of 3.0 M $KHCO_3$.

(E) Full-cell voltage as a function of time for 3.0 M $KHCO_3$ at 100 mA cm^{-2}. $KHCO_3$ was depleted after each cycle of electrolysis, yielding an average 91.33% of formate with an average of 15.62 wt % over 100 h.

(F) Plot of CO_2(aq) concentration in water as a function of CO_2 partial pressure and operating temperature.

(G) Plot of HCO_3^-(aq) concentration as a function of CO_2 partial pressure and operating temperature with a fixed alkalinity of 3.0 M. Data for plots (F) and (G) were extracted and extrapolated from Dodds et al.[28] and Saruhash.[29]

would be especially important at high current densities when the proton flux is high. In fact, the incorporation of this intermediate buffer layer would enhance the FE from around 50% to over 80% for CO_2ER with 3 M bicarbonate. We hypothesize this could be due to the favorable pH gradient induced by the buffer layer. After dissembling the cell, we measured the buffer material to be around 200 μm thickness. This thickness of layer impregnated with bicarbonate could effectively buffer the pH at the cathode surface, suppressing HER and favoring CO_2RR. A similar finding on the effect of buffer thickness was also reported recently.[33]

Enrichment of K^+(aq) in the vicinity of the catalyst surface could lead to enhanced CO_2ER selectivity due to the cation charge effect at the outer Helmholtz layer[4,34] and increased concentration of the bicarbonate reactant. We first fixed the HCO_3^-(aq) anion concentration to be 0.1 M while varying the K^+(aq) concentration, with the charge balanced by adding Cl^-(aq). There were no significant differences in neutral-pH-solution electrolysis (Figure 3C). We also investigated the impact of anions (including Cl^-, I^-, SO_4^{2-}) on the performance, and we found no obvious change either (Figure S8). Subsequently, we increased both the cation and anion concentrations, and electrolyzed a concentrated (1.0 M) $KHCO_3$ solution, which gave an astonishing 96.67% formate conversion efficiency. It was discovered that the bicarbonate feedstock of higher concentration could sustain a larger current density of 50 mA cm^{-2} until the near complete depletion of inorganic carbon feedstock (Figure 3A). Electrolysis of sodium bicarbonate feedstock in the same conditions led to slightly higher overpotential and lower FE (Figure 3B). With an even more concentrated (3.0 M) $KHCO_3$ solution, our strategy enabled an FE of formate formation of 70.74% at 100 mA cm^{-2} at 25°C (Figures 3D and S9). The MEA electrolyzer with the 3.0 M $KHCO_3$ feedstock could operate at a current density of 100 mA cm^{-2} for over 100 h, yielding over 15 wt % of potassium formate. The yield dropped slightly to an average of over 70% for the prolonged electrolysis test at large current densities (Figure 3E). For comparison, we also performed the electrochemical conversion of bicarbonate to formate in an H-type cell. While we observed similar carbon efficiency and FE compared with the MEA full cell, a lower current density at various potentials was seen (Figure S13).

We first hypothesized that this gradual decrease of carbon efficiency upon long-term testing might be due to the imbalance of CO_2 dissolution-exsolution equilibrium, which is triggered by the continuous decrease of CO_2 partial pressure with the accumulation of H_2 gas in the headspace. As we used aqueous feedstock and the catalyst sites were flooded, we modeled the CO_2 exsolution rate from the bulk bicarbonate reservoir with the Hertz-Knudsen equation.[35,36] Higher current densities led to accelerated CO_2 exsolution and the generation of carbonate (Figure S10). This issue may be addressed by incorporating a CO_2/H_2 separation membrane (e.g., Pd

membrane[37]) to *in situ* remove H_2 or by applying a higher-pressure reaction vessel to enable a higher concentration of dissolved CO_2 (Figures 3F and 3G) or both. Higher temperature results in more CO_2(g) exsolution, while higher partial pressure results in more CO_2(g) dissolution. High temperature should also expedite reaction kinetics due to the Arrhenius law if [CO_2(aq)] is controlled to be the same.

Therefore, we built a customized high-pressure MEA electrolyzer to achieve high yield for concentrated bicarbonate solution (Figure S14). Our setup allowed up to 5 bar of CO_2 partial pressure for a flow electrolyzer. The FE increased to 82.11% at 5 bar. However, we could not increase the yield above 70% for a *saturated* bicarbonate solution. Because the reaction of $H^+ + HCO_3^- \rightarrow CO_2 + H_2O$ has a larger *p*Ka (~6.36) than the formic acid dissociation constant (~3.75), there should be continuous generation and transport of CO_2(aq) to the cathode. But still, no reaction is observed beyond a certain formate/bicarbonate ratio *at high concentrations*. We thus hypothesized this could be due to the poisoning effect of formate on the electrode. At high formate concentrations, the formate anion would compete against the CO_2 for specific adsorption and therefore leads to product inhibition. In the future, catalysts that could withstand formate poisoning *at high concentrations* should be developed. These catalysts should lead to the production of concentrated pure formate from bicarbonate, thus reducing the liquid separation cost.

In addition to HCO_3^-(aq) feedstock, our CEM electrolyzer may also use high-pressure CO_2(gas) feedstock directly if it is injected into the headspace. In practice, the use of high-pressure ultra-pure CO_2 gas from $CaCO_3$ baking is energy intensive. The implication here, nevertheless, is the potential of using high-pressure flue gas directly, which will ensure high CO_2 partial pressure and also lead to high carbon efficiency per our design principle. We envision a steady-state mode of $OOCH^-$(aq) production from high partial pressure CO_2(gas) into the headspace and alkali-metal hydroxide added to balance the pH, which will enable the continuous production of highly concentrated $OOCH^-$(aq) liquor.

From the highly concentrated $OOCH^-$(aq)-bearing liquor produced, we obtained pure potassium formate (KOOCH) crystals by evaporation-induced precipitation, shown in Figure 1G and verified by X-ray diffraction (XRD) (Figure 2D). Solar evaporation can be implemented efficiently at industrial scale without significant CO_2 footprint.[38] Solid alkali-metal and alkaline-earth formates (KOOCH, NaOOCH, $Ca(OOCH)_2$, etc.) are non-toxic, stable, non-corrosive, and suitable for safe, long-term storage, over many years if necessary.[39,40] In terms of energy density, solid formate fuels are comparable volumetrically to 350-bar hydrogen tanks (Note S1). One just needs to drop such solid salts into water to power a DFFC.[27] Thus, the combination of high-efficiency bicarbonate-to-formate electrolyzer and DFFC should enable a "solid formate" economy, wherein nations mine volcanic alkali basalt rocks containing ~10 wt % K_2O/Na_2O/CaO and use the soluble components through the presented bicarbonate-formate cycle for long-term fuel generation and storage and the insoluble left-over components (MgO/SiO_2), after enhanced weathering,[25] for geological sequestration. The alkali basalt resources on Earth exceed the scale needed for the global energy transition (cycling of 60 Gt $year^{-1}$ CO_2 equivalent) and CO_2 sequestration (103 Gt CO_2) to mitigate climate change.

Direct formate fuel cells with produced formate

As a proof of concept for the "metal formate" economy, we also assembled DFFCs with our own developed catalyst and our own CO_2ER-produced formate. We prepared a palladium nanoparticle-based catalyst with a facile method of *in situ*

Please cite this article in press as: Zhang et al., A carbon-efficient bicarbonate electrolyzer, Cell Reports Physical Science (2023), https://doi.org/10.1016/j.xcrp.2023.101662

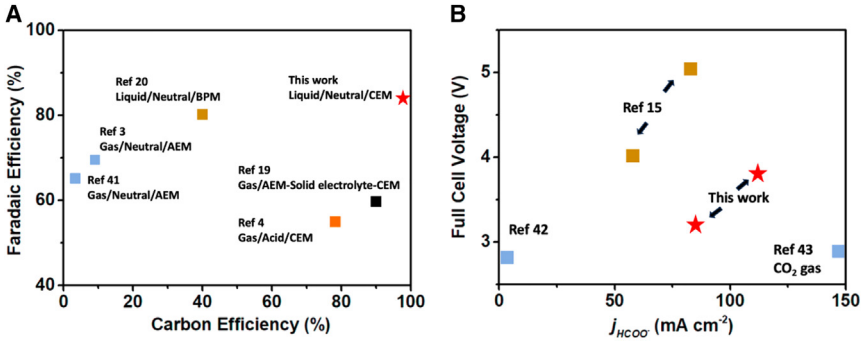

Figure 4. Comparison of figures of merit with literature

(A) Plot of Faradaic efficiency and carbon efficiency for different electrolysis systems.[3,4,19,20,44] Liquid/gas denotes a reactant feedstock of bicarbonate/CO_2, respectively. Neutral/acid denotes the pH conditions of the catholyte. Literature results with an FE of >90% using CO_2 gas feedstock were not included, because the carbon efficiency was not reported. In fact, to achieve an FE of >90% with CO_2(g), a high flow rate of CO_2 is required, which lowers the carbon efficiency enormously. For the literature cited in this plot, a CO_2(g) flow rate of ~3 sccm was typically used. (B) Plot of full-cell voltage and partial current density for formate production. All citations are for electrolysis with bicarbonate feedstock,[15,45] except the data at the lower right,[46] which is the state-of-the-art performance achieved with CO_2(g). The use of CO_2(g) leads to better performance in terms of voltage/current, but it suffers in the actual efficiency and capital cost.

electrodeposition (Figure S15). Due to the densely packed nanoparticles, our catalyst exhibited comparable performance as the commercially available catalysts in a DFFC full cell but with 4 times less the palladium loading (Figure S16).

To summarize, from captured liquid bicarbonate or saturated liquid/solid bicarbonate feedstocks, we can produce solid metal formates (crystalized KOOCH, NaOOCH) of high purity with nearly 100% carbon efficiency and decent current density at ambient pressure and temperature (Figure 4). The full-cell reaction achieved is $\Delta H_f^\circ(KHCO_3 \rightarrow KOOCH + \frac{1}{2}O_2) = 3.13$ eV,[41,42] which is highly analogous to water splitting $\Delta H_f^\circ(H_2O \rightarrow H_2 + \frac{1}{2}O_2) = 2.96$ eV,[43] with no net acid or base produced; thus the pH of both the catholyte and anolyte compartments are maintained with the use of a single CEM and a buffer layer. The dominance of a high concentration of dissolved bicarbonate over carbonate by maintaining appreciable H^+(aq) is of vital importance to achieving enhanced carbon efficiency and FE of CO_2ER, and this could be facilely implemented by near-neutral-pH anolyte, CEM, and CO_2 partial pressure management. The direct and complete conversion of highly concentrated bicarbonate liquor in mild conditions is significant to the seamless coupling of carbon dioxide capture and electroreduction. A "formate economy" is envisioned, where metal formates play the role of "solid hydrogen" that are much easier to store over decadal timescales. A DFFC that oxidizes our produced fuel and generates electricity is also demonstrated.

EXPERIMENTAL PROCEDURES

Resource availability

Lead contact

Further information and requests for resources should be directed to and will be fulfilled by the lead contact, Ju Li (liju@mit.edu).

Materials availability

The materials described in this study, except those obtained from commercial sources or third parties, can be made available upon request.

Please cite this article in press as: Zhang et al., A carbon-efficient bicarbonate electrolyzer, Cell Reports Physical Science (2023), https://doi.org/10.1016/j.xcrp.2023.101662

Data and code availability

Additional data that support the findings of this study are available from the corresponding author upon request.

Materials and methods

Chemicals and materials used for the electrode and electrolyte preparation and electrolyzer assembly, including potassium bicarbonate (≥99.95% trace metals basis), potassium hydroxide (ACS reagent, ≥85%, pellets), potassium chloride (ACS reagent, 99.0%–100.5%), potassium iodide (ACS reagent, >99%), potassium sulfate (ACS reagent, >99%), sulfuric acid (ACS reagent, 95.0%–98.0%), nitric acid (ACS reagent, 70%), multi-walled carbon nanotube (50–90 nm diameter, >95% carbon basis), Nafion 117 ionomer solution (5 wt %), Whatman GF/D microfiber filters (diameter 35 mm), were purchased from Sigma-Aldrich. Carbon substrates including Avcarb 190 carbon paper, Panex carbon cloth, and Aquivion E98-09S CEM (thickness 90 μm) were purchased from Fuel Cell Store. Tin nanoparticles (99.95%, 60–80 nm) were purchased from US Research Nanomaterials. The anode material, IrO_2 on carbon paper, was purchased from Dioxide Materials and directly used in the electrolyzer test. Deionized water (18.2 MΩ) was used for the preparation of electrolytes. Carbon substrates purchased from Fuel Cell Store were directly used as hydrophobic carbon substrates. Hydrophilic carbon substrates were obtained by immersion treatment of the carbon substrates in the concentrated nitric acid (70%) overnight (>12 h). The cathode electrodes were prepared by manually airbrushing precursor solutions on carbon substrates. For the preparation of the Sn (tin) electrodes, tin nanoparticles, multi-walled carbon nanotubes, and Nafion 117 were mixed with a weight ratio of 1:0.2:1 using pure ethanol. Note that the Nafion ionomer is 5 wt %, so that the Sn/Nafion weight ratio is 20:1 rather than 1:1. The loading density for the Sn electrodes was ~ 4 mg/cm^2. The buffer layer was prepared by immersing the Whatman glass fiber in the corresponding bicarbonate solution (at the same concentration as the catholyte). The catalyst for DFFCs was prepared by *in situ* electrodeposition. 100 μ L/cm^2 of palladium chloride solution (50 mM in ethanol) was dropcasted onto carbon strips with a robotic Opentron machine. The carbon was then immersed in a solution of potassium formate (1 M) and potassium hydroxide (1 M). A constant potential of −0.524 V vs. HgO/Hg was applied to the cathode for 5 min.

Flow cell assembly

The MEA flow electrolyzer used was purchased from Dioxide Materials. It was composed of two compartments: anolyte chamber with a titanium anode flow field and catholyte chamber with 904-L stainless-steel flow field. The size of the electrode exposed to the flow field was 5 cm^2. The buffer layer was clamped between the cathode and the CEM, with the cathode substrate side facing the catholyte flow field and catalyst side facing the buffer layer. The catholyte and anolyte were constantly flowing in and out through silicone tubes connected to peristaltic pumps, both with a constant flow rate of approximately 10 mL/min. The same catholyte/anolyte electrolyte solutions were recirculated in/out of the bulk solutions to form closed loops.

Electrochemical tests

All the electrochemical tests were carried out using an electrochemical workstation of Gamry 3000. Fresh bicarbonate solutions were prepared by dissolving potassium bicarbonate in deionized water and were used immediately. The bicarbonate solutions could also be prepared by sparging CO_2 gas (Airgas, industrial pure) into aged bicarbonate or carbonate solutions to make sure as much as carbonate is converted. Before a typical test, CO_2 gas was sparged to fill the solvent bottle

Please cite this article in press as: Zhang et al., A carbon-efficient bicarbonate electrolyzer, Cell Reports Physical Science (2023), https://doi.org/10.1016/j.xcrp.2023.101662

to drive away any air. Then the solvent bottle was closed and maintained under a constant-pressure environment throughout the test. No additional external CO_2 gas source was used in the electrolysis process. In addition, no N_2 gas was sparged in as the carrier gas. Bicarbonate solutions of various concentrations were used as the catholyte. Deionized water was typically directly used as the anolyte. There was no significant difference between using deionized water or slightly acidic water (pH ranging from 3–5 with sulfuric acid) as the anolyte. The liquid products were tested with NMR, while the gas products were tested with gas chromatography (GC) in a separate control test. The CO_2ER performances were typically tested in a flow cell assembly under the galvanostatic mode. The voltage measured and reported was the full-cell voltage, and no voltage compensation method was used. For the DFFC test, the catholyte is a mixture of potassium formate (1.0 M) and potassium hydroxide (2.0 M), while the anode feeding gas is pure O_2. The DFFC test occurred at 60°C. For the H cell test, the H-Type Sealed Electrochemical Cell (10/40 mL) was purchased from Dek Research. An Ag/AgCl electrode was used as the reference electrode.

Nuclear magnetic resonance tests

The liquid products were analyzed using ^{1}H NMR spectroscopy (400-MHz, two-channel Bruker Avance-III HD Nanobay spectrometer) with water suppression. Dimethyl sulfoxide was used as the internal standard and deuterium oxide (D_2O) as the lock solvent. The D_2O:H_2O volume ratio was 1:9. A high concentration of formate solution would be diluted before tests. The FE was calculated using the equation below:

$$\text{Faradaic efficiency}\ (\%) = N \times F \times \frac{n_{\text{product}}}{Q}, \qquad \text{(Equation 8)}$$

where N is the number of electrons transferred, F is the Faradaic constant, n_{product} is the total moles of products, and Q the total charge passed. The yield of formate was calculated below:

$$\text{Yield}\ (\%) = n_{\text{formate}} / n_0, \qquad \text{(Equation 9)}$$

where n_{formate} is the total moles of formate produced, and n_0 is the concentration of the starting solution or conservative cation (K^+).

The standard calibration curve and a typical test result are shown in Figure S4.

Gas chromatography tests

The gaseous products were analyzed using a GC instrument (SRI 8610C, Multiple Gas Analyzer #5). The instrument was equipped with a thermal conductivity detector for H_2, O_2, and N_2 analysis, a flame ionization detector (equipped with a methanizer) for CO, CO_2, and hydrocarbon analysis, two 10-port gas sampling valves, three columns including a 0.5-meter Hayesep D column, a 2-meter Hayesep D column and a 2-meter Moleseive 5A column, and a 6-channel PeakSimple USB data system. Argon gas (Airgas, ultra-pure) was used as the carrier gas. The gas products were sparged out with N_2 carrier gas and dried with a custom-made $MgSO_4$ (Sigma-Aldrich) drying vessel before the GC test. For quantification, each time, 1 mL of gaseous stream was *automatically* injected into the GC, and the performance was evaluated as follows:

$$\text{Faradaic efficiency}\ (\%) = n \times F \times v \times \frac{c}{(I \times V_m)}, \qquad \text{(Equation 10)}$$

where n is the number of electrons transferred, F the Faradaic constant, v the gas flow rate, c the concentration (in ppm) of gas product, I the total current, and V_m

the molar volume of the gas. The gas flow rate was measured with a mass flow meter at the outlet of the electrolyzer.

The standard calibration and a typical test result are shown in Figures S11 and S12.

X-ray diffraction

XRD was conducted on the X-ray diffractometer (Aeris Research edition) using a copper target under a voltage of 40 kV and current of 15 mA. The hygroscopic formate was dried completely before the XRD test.

Computation of the concentrations of inorganic carbon species in the aqueous solution in equilibrium with different atmospheres was performed.

Inorganic carbon species concentration ([IC]) dissolved in the aqueous solution is defined as the following sum:

$$[IC] = [CO_2](aq) + [HCO_3^-] + [CO_3^{2-}] \quad \text{(Equation 11)}$$

The equilibrium balance of various inorganic carbon species considered could be evaluated with the following equilibrium equations and constants:

$$CO_2(aq) \rightleftharpoons CO_2(g), H_{cp} = \frac{[CO_2](aq)}{p_{CO_2}} \quad \text{(Equation 12)}$$

$$CO_2(aq) + H_2O \rightleftharpoons HCO_3^- + OH^-, K_1 = \frac{[HCO_3^-][OH^-]}{[CO_2](aq)} \quad \text{(Equation 13)}$$

$$HCO_3^- \rightleftharpoons H^+ + CO_3^{2-}, K_2 = \frac{[H^+][CO_3^{2-}]}{[HCO_3^-]} \quad \text{(Equation 14)}$$

$$H_2O \rightleftharpoons H^+ + OH^-, K_w = [H^+][OH^-] \quad \text{(Equation 15)}$$

Here, H_{cp} is the Henry's constant and could be evaluated as 0.034 M/bar for a dilute salt solution at 1 atm and room temperature, two carbonic acid dissociation constants K_1 and K_2 were evaluated as $K_1 = 9.6 \times 10^{-7}$ M and $K_2 = 3.4 \times 10^{-10}$ M at room temperature, respectively, and the water dissociation constant K_w was 1.0×10^{-14} M^2. The partial pressure of CO_2 (p_{CO_2}) was approximated as 0.4 mbar (or 400 ppm) when the solution was in equilibrium with air or 1 bar when the solvent bottle was filled with pure CO_2, respectively. In an aqueous solution of potassium bicarbonate, the ion charge balance equation could be written as follows:

$$[K^+]+[H^+] = [HCO_3^-] + 2[CO_3^{2-}] + [OH^-] \quad \text{(Equation 16)}$$

The alkalinity [A] is defined as the concentration of the conservative ion in the solution, and thus,

$$[A] = [K^+] = [HCO_3^-] + 2[CO_3^{2-}] + [OH^-] - [H^+] \quad \text{(Equation 17)}$$

Where the concentrations of $[HCO_3^-]$, $[CO_3^{2-}]$, $[OH^-]$, and $[H^+]$ could all be written as a function of $[HCO_3^-]$, $[CO_3^{2-}]$, or $[H^+]$ from the equilibrium relations above. Thus, [A] is a function of only one variable. For example, if using the variable $[H^+]$, we could have the following:

$$[A] = H_{cp}\, p_{co_2}\left(\frac{K_1}{[H^+]} + \frac{2K_1K_2}{[H^+]^2}\right) + \frac{K_w}{[H^+]} - [H^+] \quad \text{(Equation 18)}$$

We then used Python to compute and plot the alkalinity or pH as a function of the inorganic carbon species (Figures 1E, 1F, and S3).

Computation of the decline of aqueous CO_2 concentration as a function of time at different current densities due to partial pressure drop

As the electrolysis was carried out under the constant-pressure condition, pCO_2 would continuously decline while p_{H_2} increases. The Hertz-Knudsen equation could be written in the form:

$$R_{ex,CO_2} = \frac{1}{A}\frac{dN}{dt} = \frac{\alpha \Delta p N_A}{\sqrt{2\pi MRT}} = ak_{GL} \Big/ V_0\left([CO_2](aq) - [CO_2]_{eq}\right) \quad \text{(Equation 19)}$$

Here, R_{ex,CO_2} is the rate of CO_2 dissolution/exsolution from the solution with a unit of mole/time. R_{ex,CO_2} would be negative/positive for CO_2 dissolution/exsolution, respectively. a is the interfacial area with a unit of m^2/m^3. k_{GL} is the gas-to-liquid mass transfer coefficient with a unit of m/s. V_0 is the solution volume with a unit of m^3.

Reaction kinetics could be considered with the following equations:

$$CO_2(aq) + H_2O \rightleftharpoons HCO_3^- + OH^-, K_1 = \frac{k_1}{k_{-1}} \quad \text{(Equation 20)}$$

$$HCO_3^- \rightleftharpoons H^+ + CO_3^{2-}, K_2 = \frac{k_2}{k_{-2}}, \quad \text{(Equation 21)}$$

where k_n and k_{-n} refer to the rate constant of the forward and reverse reaction, respectively. The reactions of OH^- with inorganic carbon species were neglected at this point, because the pH was constant and neutral throughout the process. We only approximated the $[CO_2]$ change in the bulk solution due to the partial pressure change. The rate of $[CO_2]$ change could be written as follows:

$$\frac{d[CO_2](aq)}{dt} = -R_{ex,CO_2} + k_{-1}[HCO_3^-][H^+] \quad \text{(Equation 22)}$$

The results are shown in Figure S10.

SUPPLEMENTAL INFORMATION

Supplemental information can be found online at https://doi.org/10.1016/j.xcrp.2023.101662.

ACKNOWLEDGMENTS

We extend gratitude to Alexander Quinn for the design of the high-pressure flow electrolyzer with sealed reservoirs for this work. We thank Y. Huang, H. Tang, and A. Abdelhafiz for helpful discussions and S. Miao for graphics design. This work was supported as part of the Hydrogen in Energy and Information Sciences (HEISs), an Energy Frontier Research Center funded by the US Department of Energy (DOE), Office of Science, Basic Energy Sciences (BES), under award DE-SC0023450.

AUTHOR CONTRIBUTIONS

Conceptualization, J.L. and Z.Z.; methodology, J.L. and Z.Z.; investigation, J.L., Z.Z., D.X., and Z.R.; writing – original draft, Z.Z.; writing – review & editing, J.L., Z.Z., D.X., and Z.R.; funding acquisition, J.L.; resources, J.L. and Z.Z.; supervision, J.L.

DECLARATION OF INTERESTS

J.L. and Z.Z. from Massachusetts Institute of Technology filed a provisional patent application for high-yield production of formate salts from bicarbonate using the pressure and pH control method.

Received: July 19, 2023
Revised: September 5, 2023
Accepted: October 5, 2023
Published: October 30, 2023

REFERENCES

1. Francke, R., Schille, B., and Roemelt, M. (2018). Homogeneously Catalyzed Electroreduction of Carbon Dioxide-Methods, Mechanisms, and Catalysts. Chem. Rev. *118*, 4631–4701. https://doi.org/10.1021/acs.chemrev.7b00459.

2. Ross, M.B., De Luna, P., Li, Y., Dinh, C.-T., Kim, D., Yang, P., and Sargent, E.H. (2019). Designing materials for electrochemical carbon dioxide recycling. Nat. Catal. *2*, 648–658. https://doi.org/10.1038/s41929-019-0306-7.

3. García de Arquer, F.P., Dinh, C.-T., Ozden, A., Wicks, J., McCallum, C., Kirmani, A.R., Nam, D.-H., Gabardo, C., Seifitokaldani, A., Wang, X., et al. (2020). CO_2 electrolysis to multicarbon products at activities greater than 1 A cm^{-2}. Science *367*, 661–666. https://doi.org/10.1126/science.aay4217.

4. Huang, J.E., Li, F., Ozden, A., Sedighian Rasouli, A., García de Arquer, F.P., Liu, S., Zhang, S., Luo, M., Wang, X., Lum, Y., et al. (2021). CO_2 electrolysis to multicarbon products in strong acid. Science *372*, 1074–1078. https://doi.org/10.1126/science.abg6582.

5. Rosen, B.A., Salehi-Khojin, A., Thorson, M.R., Zhu, W., Whipple, D.T., Kenis, P.J.A., and Masel, R.I. (2011). Ionic Liquid–Mediated Selective Conversion of CO_2 to CO at Low Overpotentials. Science *334*, 643–644. https://doi.org/10.1126/science.1209786.

6. Lees, E.W., Mowbray, B.A.W., Parlane, F.G.L., and Berlinguette, C.P. (2021). Gas diffusion electrodes and membranes for CO_2 reduction electrolysers. Nat. Rev. Mater. *7*, 55–64. https://doi.org/10.1038/s41578-021-00356-2.

7. Azcarate, I., Costentin, C., Robert, M., and Savéant, J.M. (2016). Through-Space Charge Interaction Substituent Effects in Molecular Catalysis Leading to the Design of the Most Efficient Catalyst of CO_2-to-CO Electrochemical Conversion. J. Am. Chem. Soc. *138*, 16639–16644. https://doi.org/10.1021/jacs.6b07014.

8. Rabinowitz, J.A., and Kanan, M.W. (2020). The future of low-temperature carbon dioxide electrolysis depends on solving one basic problem. Nat. Commun. *11*, 5231. https://doi.org/10.1038/s41467-020-19135-8.

9. Ozden, A., Arquer, F.P.G. de, Huang, J.E., Wicks, J., Sisler, J., Miao, R.K., O'Brien, C.P., Lee, G., Wang, X., Ip, A.H., et al. (2022). Carbon-efficient carbon dioxide electrolysers. Nat. Sustain. 1–11. https://doi.org/10.1038/s41893-022-00879-8.

10. Sullivan, I., Goryachev, A., Digdaya, I.A., Li, X., Atwater, H.A., Vermaas, D.A., and Xiang, C. (2021). Coupling electrochemical CO_2 conversion with CO_2 capture. Nat. Catal. *4*, 952–958. https://doi.org/10.1038/s41929-021-00699-7.

11. Li, S., Liu, L., Li, T., Lan, T., Wang, Y., Zhang, Z., Liu, J., Xu, S., Zhang, X., Zhu, J., et al. (2019). Electrolytic Conversion of Bicarbonate into CO in a Flow Cell. Joule *132*, 1487–1503. https://doi.org/10.1016/j.joule.2019.05.021.

12. Fink, A.G., Lees, E.W., Zhang, Z., Ren, S., Delima, R.S., and Berlinguette, C.P. (2021). Impact of Alkali Cation Identity on the Conversion of HCO_3^- to CO in Bicarbonate Electrolyzers. Chemelectrochem *8*, 2094–2100. https://doi.org/10.1002/celc.202100408.

13. Keith, D.W., Holmes, G., St Angelo, D., and Heidel, K. (2018). A Process for Capturing CO_2 from the Atmosphere. Joule *2*, 1573–1594. https://doi.org/10.1016/j.joule.2018.05.006.

14. Wuttig, A., Yoon, Y., Ryu, J., and Surendranath, Y. (2017). Bicarbonate Is Not a General Acid in Au-Catalyzed CO_2 Electroreduction. J. Am. Chem. Soc. *139*, 17109–17113. https://doi.org/10.1021/jacs.7b08345.

15. Li, T., Lees, E.W., Zhang, Z., and Berlinguette, C.P. (2020). Conversion of Bicarbonate to Formate in an Electrochemical Flow Reactor. ACS Energy Lett. *5*, 2624–2630. https://doi.org/10.1021/acsenergylett.0c01291.

16. Lamaison, S., and Wakerley, D. (2022). Don't cross the streams. Nat. Catal. *5*, 242–243. https://doi.org/10.1038/s41929-022-00774-7.

17. Dunwell, M., Lu, Q., Heyes, J.M., Rosen, J., Chen, J.G., Yan, Y., Jiao, F., and Xu, B. (2017). The Central Role of Bicarbonate in the Electrochemical Reduction of Carbon Dioxide on Gold. J. Am. Chem. Soc. *139*, 3774–3783. https://doi.org/10.1021/jacs.6b13287.

18. Salvatore, D.A., Gabardo, C.M., Reyes, A., O'Brien, C.P., Holdcroft, S., Pintauro, P., Bahar, B., Hickner, M., Bae, C., Sinton, D., et al. (2021). Designing anion exchange membranes for CO_2 electrolysers. Nat. Energy *6*, 339–348. https://doi.org/10.1038/s41560-020-00761-x.

19. Kim, J.Y.', Zhu, P., Chen, F.-Y., Wu, Z.-Y., Cullen, D.A., and Wang, H. (2022). Recovering carbon losses in CO2 electrolysis using a solid electrolyte reactor. Nat. Catal. *5*, 288–299. https://doi.org/10.1038/s41929-022-00763-w.

20. Zhang, Z., Lees, E.W., Ren, S., Mowbray, B.A.W., Huang, A., and Berlinguette, C.P. (2022). Conversion of Reactive Carbon Solutions into CO at Low Voltage and High Carbon Efficiency. ACS Cent. Sci. *8*, 749–755. https://doi.org/10.1021/acscentsci.2c00329.

21. Lees, E.W., Liu, A., Bui, J.C., Ren, S., Weber, A.Z., and Berlinguette, C.P. (2022). Electrolytic Methane Production from Reactive Carbon Solutions. ACS Energy Lett. *7*, 1712–1718. https://doi.org/10.1021/acsenergylett.2c00283.

22. Li, Y.C., Lee, G., Yuan, T., Wang, Y., Nam, D.-H., Wang, Z., García de Arquer, F.P., Lum, Y., Dinh, C.-T., Voznyy, O., and Sargent, E.H. (2019). CO_2 Electroreduction from Carbonate Electrolyte. ACS Energy Lett. *4*, 1427–1431. https://doi.org/10.1021/acsenergylett.9b00975.

23. Rinberg, A., Bergman, A.M., Schrag, D.P., and Aziz, M.J. (2021). Alkalinity Concentration Swing for Direct Air Capture of Carbon Dioxide. ChemSusChem *14*, 4439–4453. https://doi.org/10.1002/cssc.202100786.

24. Jin, S., Wu, M., Jing, Y., Gordon, R.G., and Aziz, M.J. (2022). Low energy carbon capture via electrochemically induced pH swing with electrochemical rebalancing. Nat. Commun. *13*, 2140. https://doi.org/10.1038/s41467-022-29791-7.

25. McQueen, N., Kelemen, P., Dipple, G., Renforth, P., and Wilcox, J. (2020). Ambient weathering of magnesium oxide for CO_2 removal from air. Nat. Commun. *11*, 3299. https://doi.org/10.1038/s41467-020-16510-3.

26. Goll, D.S., Ciais, P., Amann, T., Buermann, W., Chang, J., Eker, S., Hartmann, J., Janssens, I., Li, W., Obersteiner, M., et al. (2021). Potential CO_2 removal from enhanced weathering by ecosystem responses to powdered rock. Nat. Geosci. *14*, 545–549. https://doi.org/10.1038/s41561-021-00798-x.

27. An, L., and Chen, R. (2016). Direct formate fuel cells: A review. J. Power Sources *320*, 127–139. https://doi.org/10.1016/j.jpowsour.2016.04.082.

28. Dodds, W.S., Stutzman, L.F., and Sollami, B.J. (1956). Carbon Dioxide Solubility in Water. Ind. Eng. Chem. Chem. Eng. Data Series *1*, 92–95. https://doi.org/10.1021/i460001a018.

29. Saruhashi, K. (1955). On the Equilibrium Concentration Ratio of Carbonic Acid Substances Dissolved in Natural Water. Pap. Met. Geophy. *6*, 38–55. https://doi.org/10.2467/mripapers1950.6.1_38.

30. Wakerley, D., Lamaison, S., Wicks, J., Clemens, A., Feaster, J., Corral, D., Jaffer, S.A., Sarkar, A., Fontecave, M., Duoss, E.B., et al. (2022). Gas

diffusion electrodes, reactor designs and key metrics of low-temperature CO_2 electrolysers. Nat. Energy *7*, 130–143. https://doi.org/10.1038/s41560-021-00973-9.

31. Lees, E.W., Goldman, M., Fink, A.G., Dvorak, D.J., Salvatore, D.A., Zhang, Z., Loo, N.W.X., and Berlinguette, C.P. (2020). Electrodes Designed for Converting Bicarbonate into CO. ACS Energy Lett. *5*, 2165–2173. https://doi.org/10.1021/acsenergylett.0c00898.

32. Delacourt, C., Ridgway, P.L., Kerr, J.B., and Newman, J. (2008). Design of an Electrochemical Cell Making Syngas (CO + H_2) from CO_2 and H_2O Reduction at Room Temperature. J. Electrochem. Soc. *155*, B42–B49. https://doi.org/10.1149/1.2801871.

33. Lee, G., Rasouli, A.S., Lee, B.-H., Zhang, J., Won, D.H., Xiao, Y.C., Edwards, J.P., Lee, M.G., Jung, E.D., Arabyarmohammadi, F., et al. (2023). CO_2 electroreduction to multicarbon products from carbonate capture liquid. Joule *7*, 1277–1288. https://doi.org/10.1016/j.joule.2023.05.003.

34. Gu, J., Wang, X., Chen, Y., Xu, K., Yu, D., and Wu, H. (2022). Modulating electric field distribution by alkali cations for CO_2 electroreduction in strongly acidic medium. Nat. Catal. *20*, 268–276. https://doi.org/10.1038/s41929-022-00761-y.

35. Wen, G., Ren, B., Wang, X., Luo, D., Dou, H., Zheng, Y., Gao, R., Gostick, J., Yu, A., and Chen, Z. (2022). Continuous CO_2 electrolysis using a CO_2 exsolution-induced flow cell. Nat. Energy *7*, 978–988. https://doi.org/10.1038/s41560-022-01130-6.

36. Ndiaye, M., Gadoin, E., and Gentric, C. (2018). CO_2 gas–liquid mass transfer and k_La estimation: Numerical investigation in the context of airlift photobioreactor scale-up. Chem. Eng. Res. Des. *133*, 90–102. https://doi.org/10.1016/j.cherd.2018.03.001.

37. Sholl, D.S., and Ma, Y.H. (2006). Dense Metal Membranes for the Production of High-Purity Hydrogen. MRS Bull. *31*, 770–773. https://doi.org/10.1557/mrs2006.191.

38. Dang, C., Wang, H., Cao, Y., Shen, J., Zhang, J., Lv, L., Xu, G., and Zhu, M. (2022). Ultra salt-resistant solar desalination system via large-scale easy assembly of microstructural units. Energy Environ. Sci. *15*, 5405–5414. https://doi.org/10.1039/d2ee03341k.

39. Gage, S., Sharan, P., Turchi, C., and Netter, J. (2021). Evaluation of Formate Salt PCM's for Latent Heat Thermal Energy Storage. Energies *14*, 765. https://doi.org/10.3390/en14030765.

40. Eggert, G., and Fischer, A. (2021). The formation of formates: a review of metal formates on heritage objects. Herit. Sci. *9*, 26. https://doi.org/10.1186/s40494-021-00499-z.

41. Wagman, D., Evans, H., Parker, B., Schumm, H., and Nuttall, L. (1981). Selected Values of Chemical Thermodynamic Properties: Compounds of Uranium, Protactinium, Thorium, Actinium, and the Alkali Metals. Final report. United States: N. p. https://www.osti.gov/biblio/5532815.

42. Lide, D. (2009). CRC Handbook of Chemistry and Physics, 90th Edition (Taylor & Francis). https://doi.org/10.1021/ja906434c.

43. National Institute of Standards and Technology (NIST). (2001). NIST Chemistry WebBook, NIST Standard Reference Database Number 69.

44. Dinh, C.-T., Burdyny, T., Kibria, M.G., Seifitokaldani, A., Gabardo, C.M., García de Arquer, F.P., Kiani, A., Edwards, J.P., De Luna, P., Bushuyev, O.S., et al. (2018). CO_2 electroreduction to ethylene via hydroxide-mediated copper catalysis at an abrupt interface. Science *360*, 783–787. https://doi.org/10.1126/science.aas9100.

45. Min, X., and Kanan, M.W. (2015). Pd-Catalyzed Electrohydrogenation of Carbon Dioxide to Formate: High Mass Activity at Low Overpotential and Identification of the Deactivation Pathway. J. Am. Chem. Soc. *137*, 4701–4708. https://doi.org/10.1021/ja511890h.

46. Xia, C., Zhu, P., Jiang, Q., Pan, Y., Liang, W., Stavitski, E., Alshareef, H.N., and Wang, H. (2019). Continuous production of pure liquid fuel solutions via electrocatalytic CO_2 reduction using solid-electrolyte devices. Nat. Energy *4*, 776–785. https://doi.org/10.1038/s41560-019-0451-x.

Cell Reports Physical Science, Volume *4*

Supplemental information

A carbon-efficient bicarbonate electrolyzer

Zhen Zhang, Dawei Xi, Zhichu Ren, and Ju Li

Supplemental Information

Supplementary Note S1

The standard Toyota Mirai hydrogen tanks volume is ~ 122 liters, storing 70 MPa of H_2. The density of sodium formate (NaOOCH) is about 1.92 g/cm^3. Thus, the mole fraction of H_2 and NaOOCH stored in this commercial tank would be 0.80. As fuel cells involving both materials are two-electron-transfer reactions, the volumetric energy density would be around 0.80.

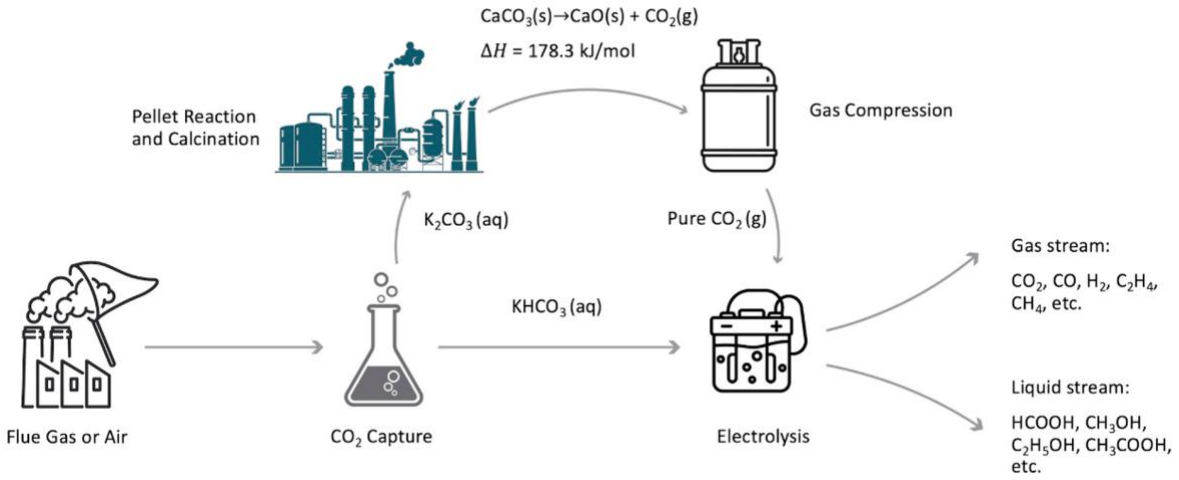

Fig. S1. Two pathways of CO_2ER using the CO_2 gas feedstock or aqueous bicarbonate feedstock. The decoupling of the carbon capture and CO_2ER processes and the demand for a pure CO_2 feedstock necessitates an energy-intensive thermal regeneration process.

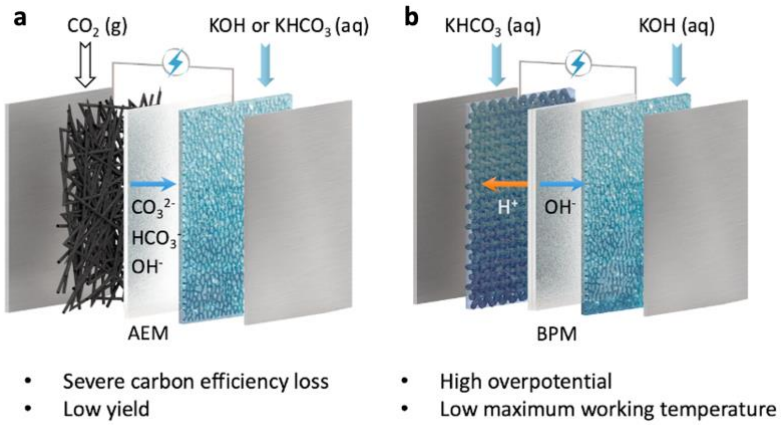

Fig. S2. (a) Schematic of the traditional anion exchange membrane (AEM) electrolyzer using the CO_2 gas feedstock. (b) Schematic of the bipolar membrane (BPM) electrolyzer using the liquid bicarbonate feedstock.

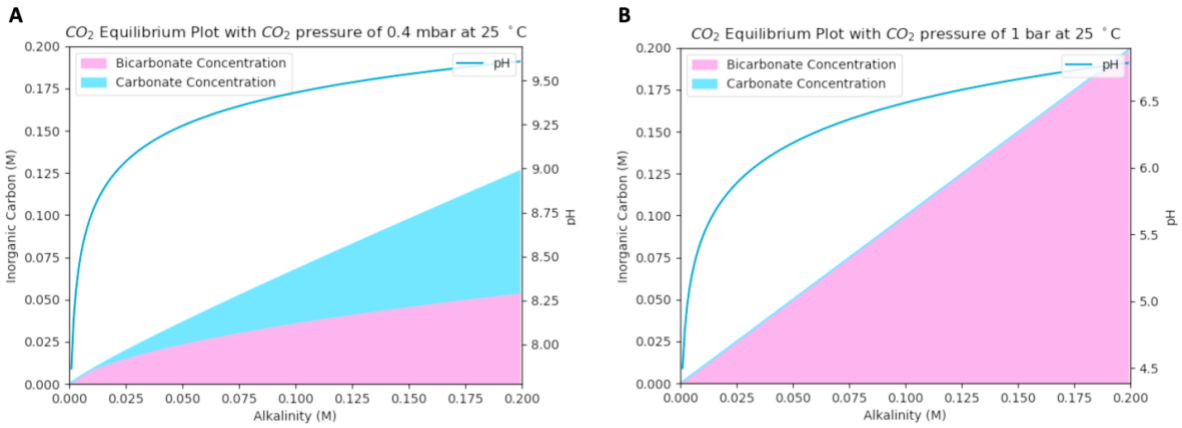

Fig. S3. The concentrations of inorganic carbon (HCO_3^-/CO_3^{2-}) and *p*H as a function of alkalinity in equilibrium with a CO_2 partial pressure of (C) 0.4 mbar and (D) 1 bar, respectively. Plum and light sky-blue areas correspond to the HCO_3^- and CO_3^{2-} concentration, respectively. This is a magnification of Fig. 2e, f at smaller concentrations.

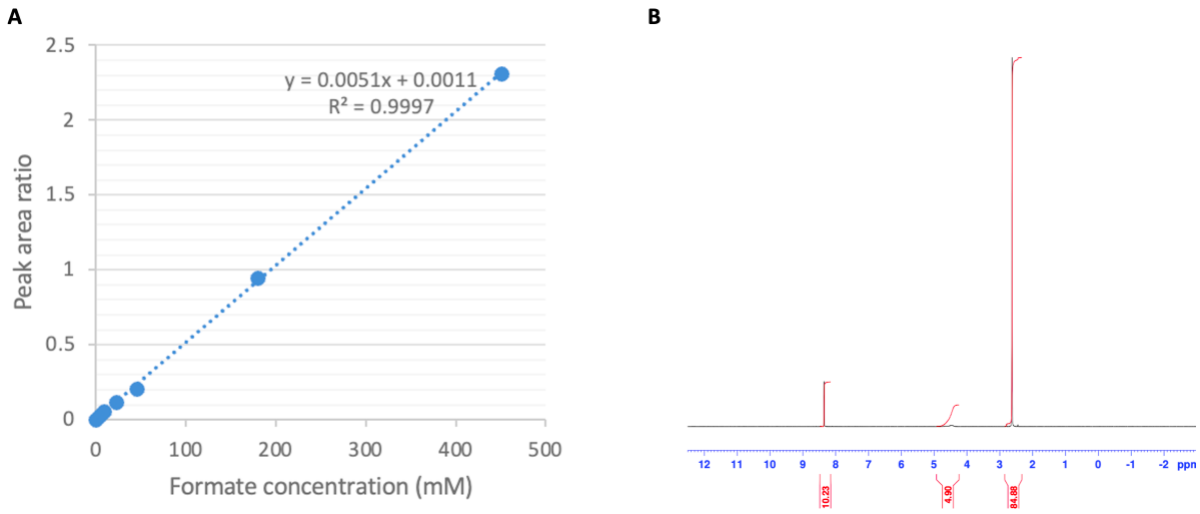

Fig. S4. Calibration curve of the potassium formate solution quantified with NMR. (a) Plot of peak area ratio as a function of formate concentration. (b) A typical NMR plot showing formate is the only liquid product. The sharp peaks at 2.63 ppm and 8.36 ppm correspond to DMSO and formate, respectively. The broad peak at 4.43 ppm results from water suppression.

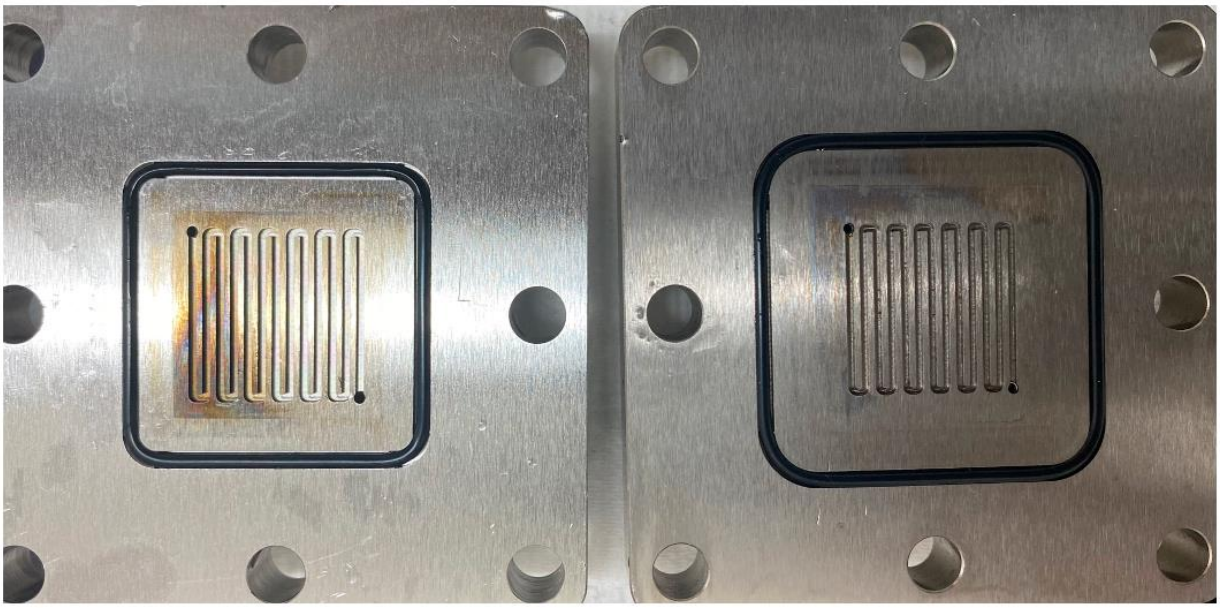

Fig. S5. The flow field of a 5 cm^2 membrane electrode assembly electrolyzer.

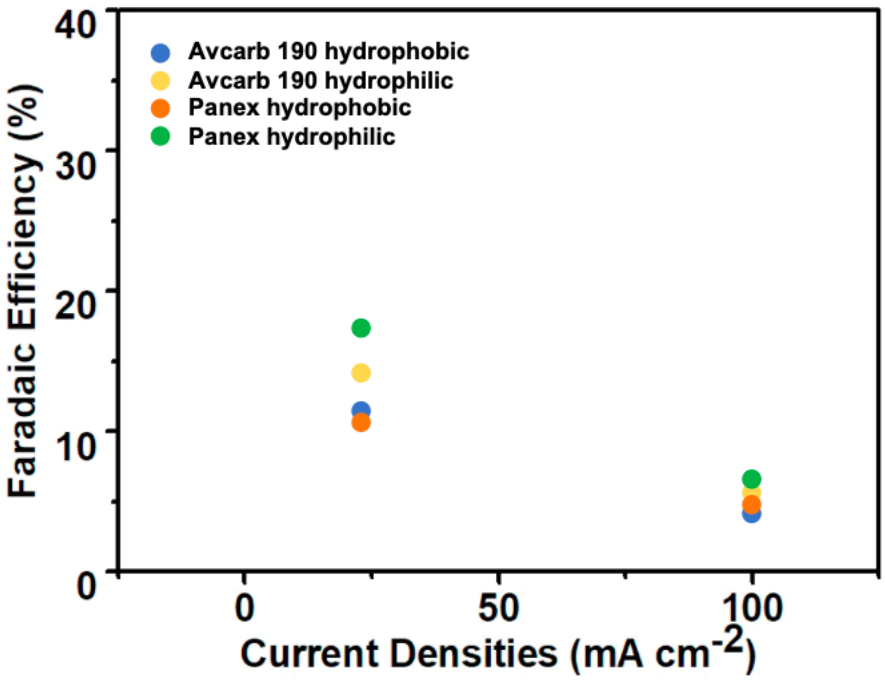

Fig. S6. Comparison of different carbon substrates for formate production. Hydrophilic substrates were acid etched to become hydrophilic samples. Avcarb 190 is basic carbon paper, while Panex is carbon cloth. The catholyte used was 0.1 M $KHCO_3$. The tests were conducted at 25 ℃.

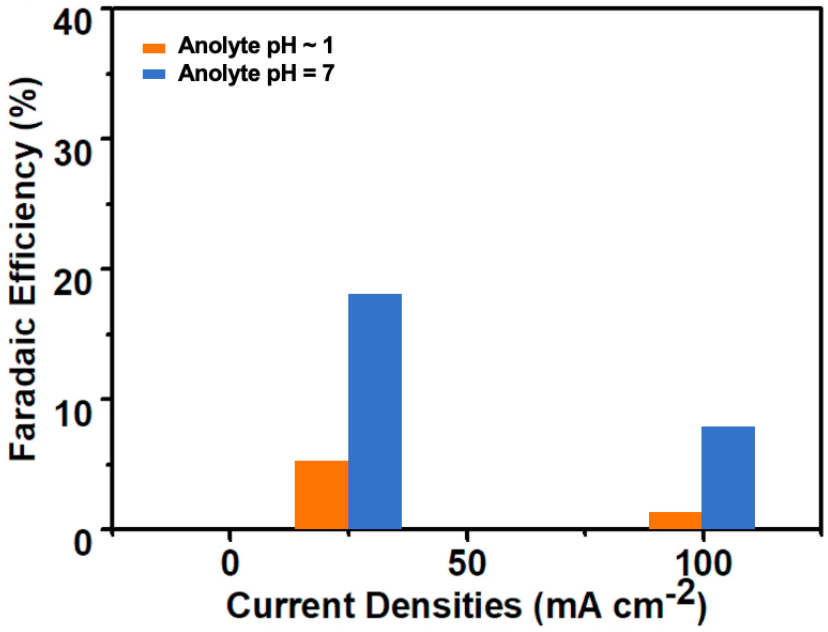

Fig. S7. Comparison of electrolysis with an anolyte of strong acid or deionized water. Sulfuric acid was used as the anolyte for the acidic electrolyte, while deionized water was directly used for the neutral electrolyte. The catholyte used was 0.1 M $KHCO_3$. The tests were conducted at 25 ℃.

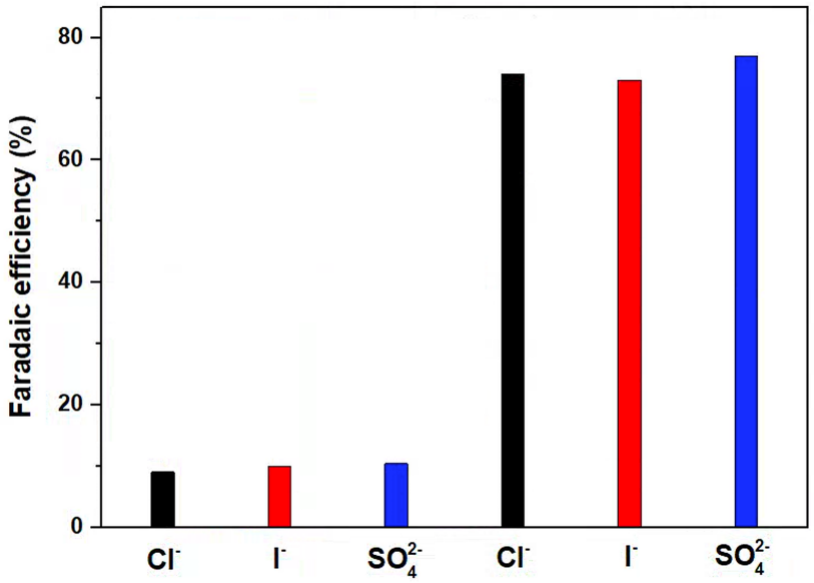

Fig. S8. Effect of anion on the Faradaic efficiency of bicarbonate conversion to formate at 100 mA/cm^2 in the MEA cell. The left three columns were performed with 0.1 M $KHCO_3$+ 0.1 M KX (X = Cl^-, I^-, ½ SO_4^{2-}). The right three columns were performed with 2.9 M $KHCO_3$+ 0.1 M KX (X = Cl^-, I^-, ½ SO_4^{2-}). No significant impact of anion was found in this reaction.

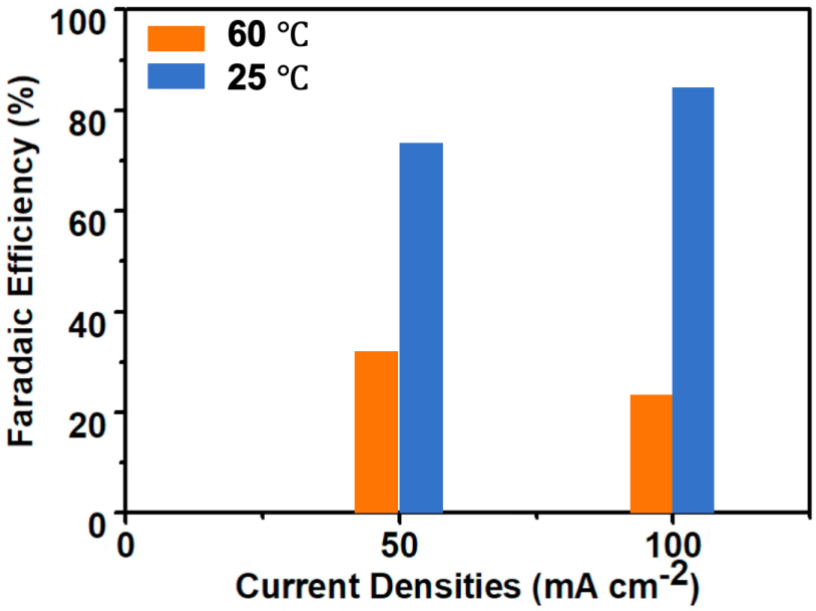

Fig. S9. Electrochemical performance conducted at different temperatures. The catholyte used was 3.0 M $KHCO_3$. There was no significant difference between the full-cell voltage at these two temperatures, which is contrary to the traditional belief that elevated temperature enhanced performance. The reason should be ascribed to a much fast CO_2 exsolution from the solution at elevated temperatures, which enormously reduced the concentration of active inorganic carbon species in the solution. However, as high temperature increased the solubility of bicarbonate, further efforts could be devoted to applying a high temperature and high-pressure strategy at the same time, which should be promising for further performance enhancement.

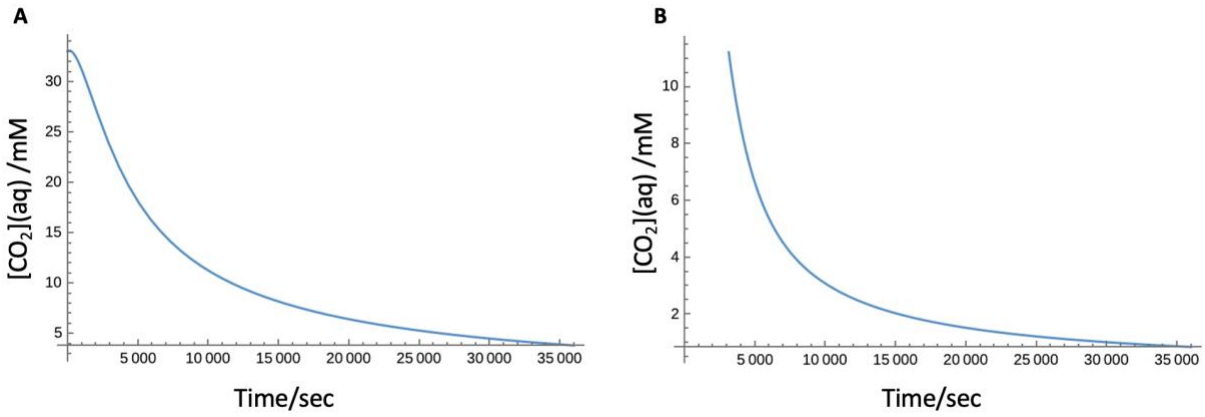

Fig. S10. Kinetics of CO_2 exsolution from the aqueous solution with the increase of hydrogen partial pressure at a current density of (a) 20 mA cm^{-2} and (b) 100 mA cm^{-2}. As CO_2 evaporated into the headspace via a flat surface from the bulk solution, we assumed a ak_{GL} at an order of magnitude of 10^{-3}. We assumed a constant faradaic efficiency for hydrogen production as 40%, bicarbonate electrolyte volume of 20 mL, solvent bottle headspace of 20 mL. Dissolved carbon dioxide concentration at equilibrium was around 33 mM, which declined much faster at a larger current density.

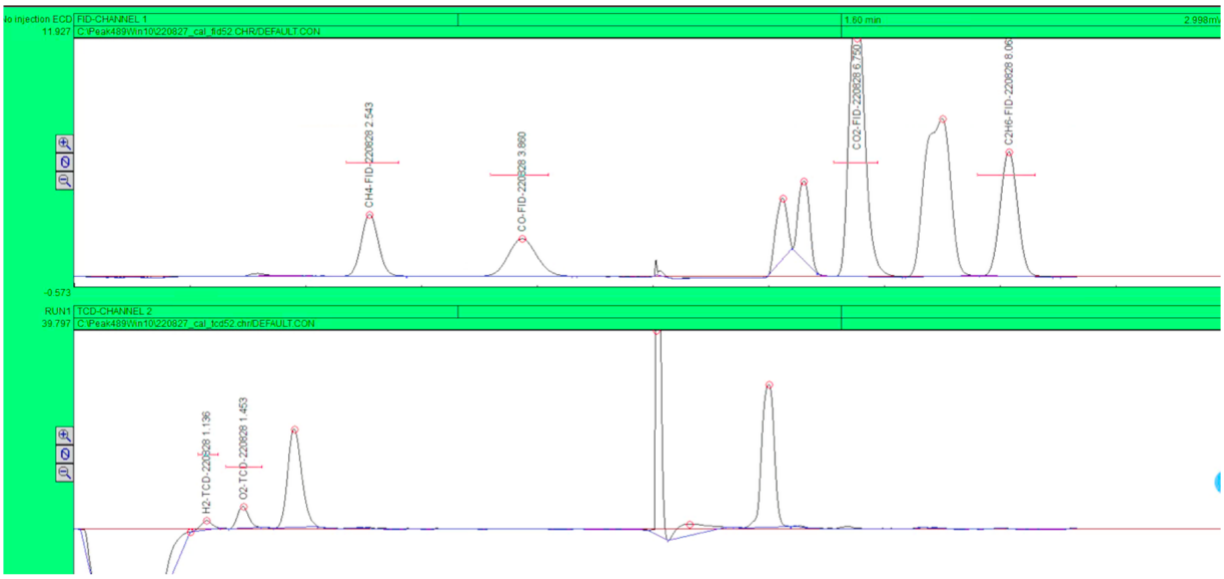

Fig. S11. Calibration curve of the gas chromatography. We only targeted at hydrogen, oxygen, carbon monoxide, methane, ethane in these experiments.

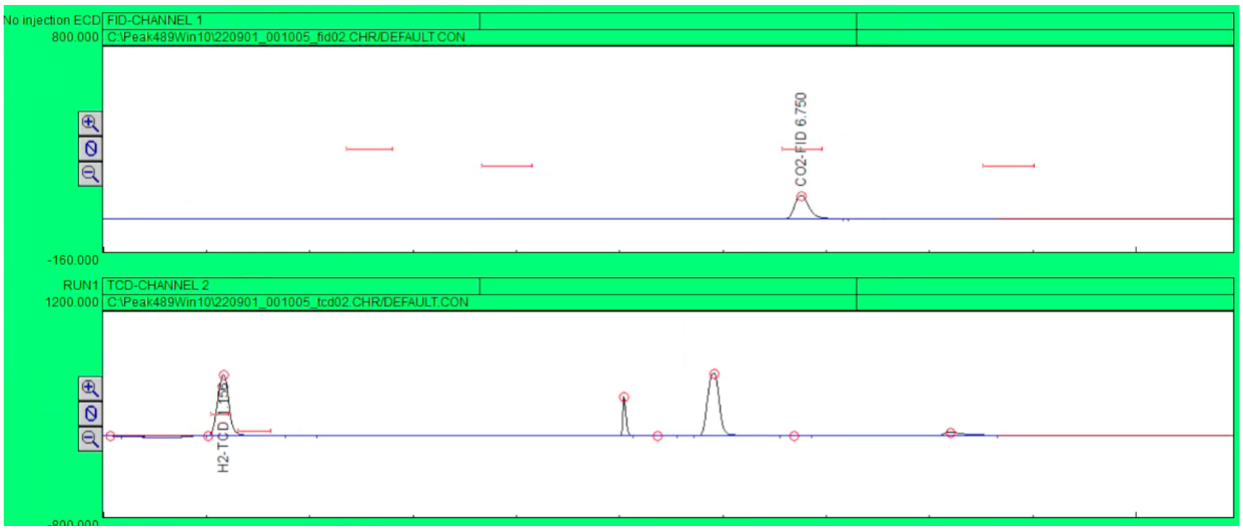

Fig. S12. A typical GC curve showing that only hydrogen and carbon dioxide were detected. Similar to the calibration plot in fig. S11, the other two peaks in the TCD curve could be ascribed to a change of valve and a second appearance of the hydrogen or air streams due to quantification by different GC columns (there were 3 columns in total), which was confirmed by the manufacturer. CO_2 appeared in the outlet because in the *control* experiments, the system was *not* closed. Nitrogen gas was constantly sparged in to drive away any gas streams evolved from the solution. However, as we stated in the main text, the system was closed under constant pressure environment for main experiments, which is the key to ensuring a high yield and high carbon efficiency. Nitrogen gas or air atmosphere would lead to an ultra-low CO_2 partial pressure, which would kill the reaction very soon.

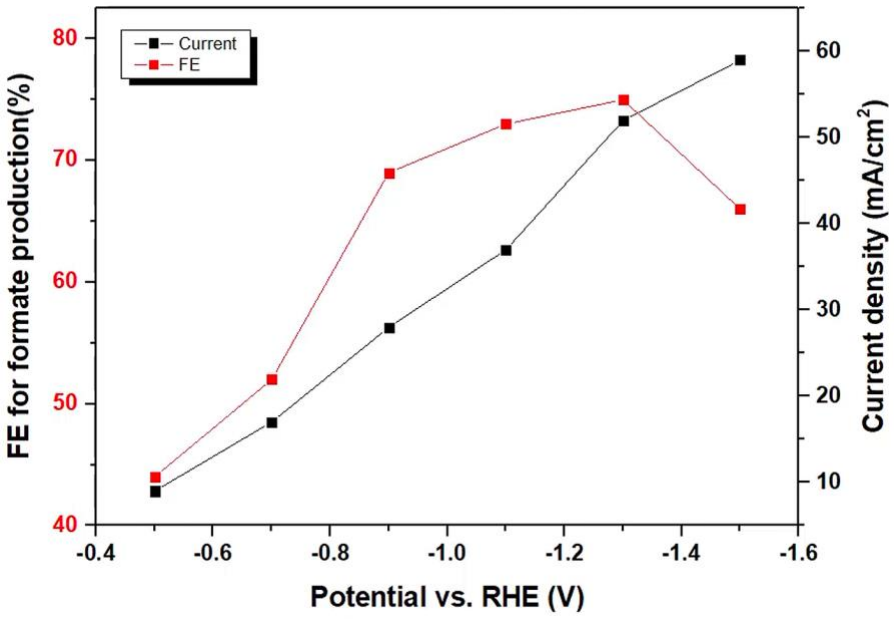

Fig. S13. Faradaic efficiency for formate production and current density as a function of electrochemical potential in an H cell. Ag/AgCl electrode was used as the reference electrode. We used 3.0 M saturated potassium bicarbonate as the catholyte, Aquivion E98-09S cation exchange membrane, and water as the anolyte.

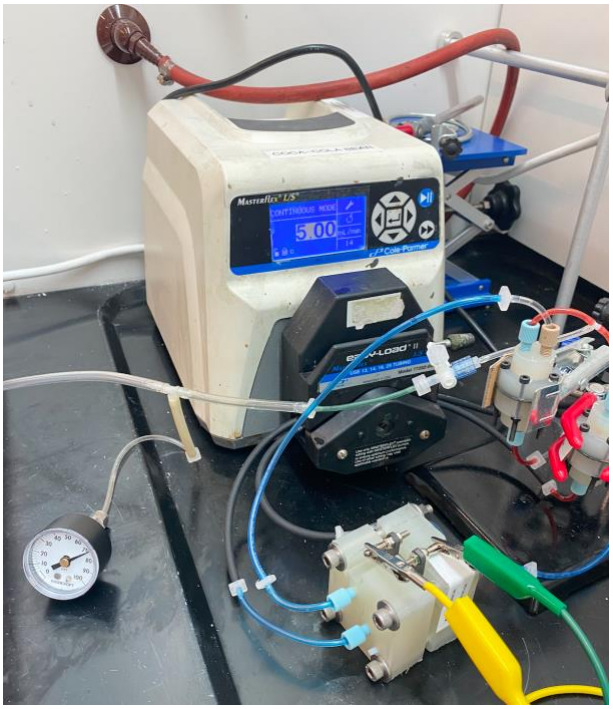

Fig. S14. Customized setup for tests up to 72 psi at MEA level. Two reservoirs were designed for holding the catholyte and anolyte, respectively, in a closed manner.

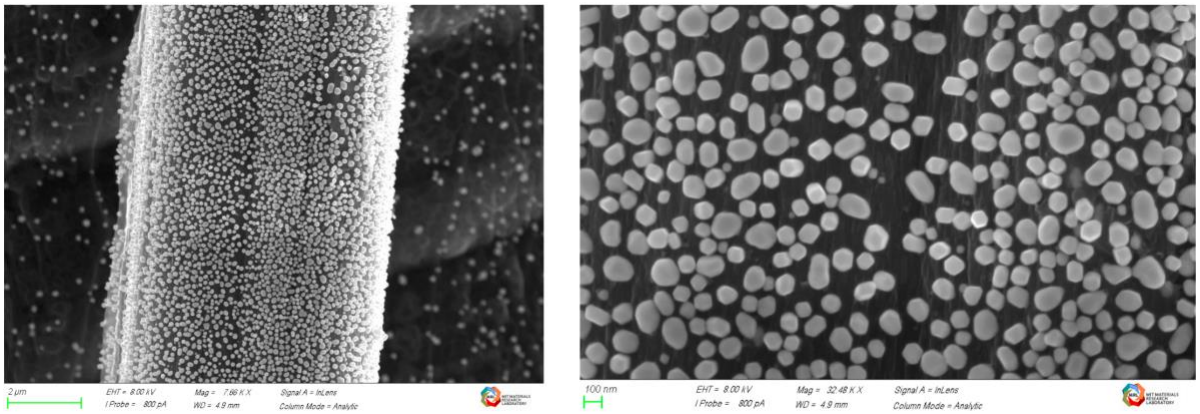

Fig. S15. Palladium nanoparticle catalyst for direct formate fuel cells, developed by in situ electrodeposition.

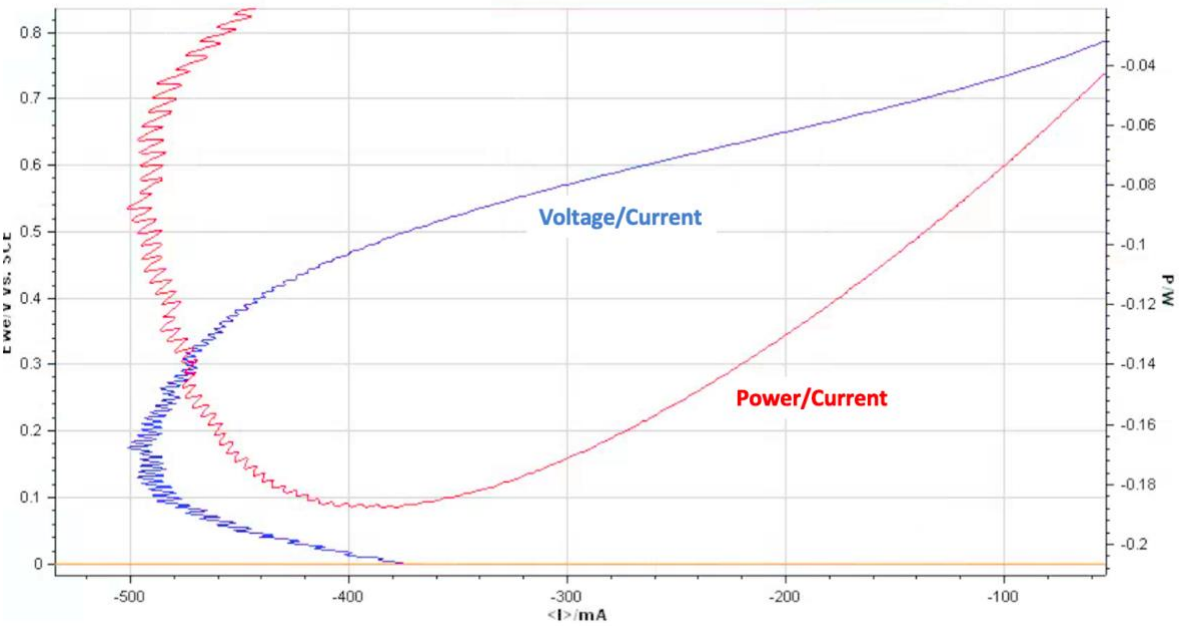

Fig. S16. Preliminary results of direct formate fuel cells at MEA level. We obtained comparable results with commercial catalysts, but with much less loading of palladium.

Table S1.

Carbon efficiency and maximum yield for different carbon dioxide electroreduction reactions.

Reactions	Maximal carbon efficiency
$2H_2O + 2e^- \rightarrow H_2 + 2OH^-$	0% (would consume CO_2)
$CO_2 + H^+ + 2e^- \rightarrow HCOO^-$	67%
$CO_2 + 2H^+ + 2e^- \rightarrow CO + H_2O$	50%
$2CO_2 + 7H^+ + 8e^- \rightarrow CH_3COO^- + 2H_2O$	36%
$CO_2 + 6H^+ + 6e^- \rightarrow CH_3OH + H_2O$	25%
$2CO_2 + 12H^+ + 12e^- \rightarrow C_2H_4 + 4H_2O$	25%
$2CO_2 + 12H^+ + 12e^- \rightarrow C_2H_5OH + 3H_2O$	25%
$CO_2 + 8H^+ + 8e^- \rightarrow CH_4 + 2H_2O$	20%

This chart shows the maximal carbon efficiency for CO_2ER with a traditional AEM-based electrolyzer. Aqueous bicarbonate feedstock coupled with a CEM could ensure 100% yield and carbon efficiency for $HCOO^-$ and oxalate production. For other products, CO_2 gas coupled with a CEM could ensure a theoretical yield of 100% as well, even though with considerable CO_2 regeneration cost with the current technology. Achieving a high yield of other products with liquid bicarbonate feedstock could be possible if an additional proton source could be realized, which would maintain *p*H balance throughout the entire process, eliminating a need for post liquid-liquid separation.